

This is a repository copy of *TIME FOR COFFEE regulates phytochrome A-mediated hypocotyl growth through dawn-phased signaling*.

White Rose Research Online URL for this paper:

<https://eprints.whiterose.ac.uk/187017/>

Version: Accepted Version

Article:

Wang, Yan, Su, Chen, Yu, Yingjun et al. (9 more authors) (2022) TIME FOR COFFEE regulates phytochrome A-mediated hypocotyl growth through dawn-phased signaling. *The Plant Cell*. 2907–2924. ISSN 1532-298X

<https://doi.org/10.1093/plcell/koac138>

Reuse

Items deposited in White Rose Research Online are protected by copyright, with all rights reserved unless indicated otherwise. They may be downloaded and/or printed for private study, or other acts as permitted by national copyright laws. The publisher or other rights holders may allow further reproduction and re-use of the full text version. This is indicated by the licence information on the White Rose Research Online record for the item.

Takedown

If you consider content in White Rose Research Online to be in breach of UK law, please notify us by emailing eprints@whiterose.ac.uk including the URL of the record and the reason for the withdrawal request.

RESEARCH ARTICLE

TIME FOR COFFEE regulates phytochrome A-mediated hypocotyl growth through dawn-phased signaling

Yan Wang^{1,2,#}, Chen Su^{1,2,#}, Yingjun Yu^{1,2,#}, Yuqing He^{1,2}, Hua Wei^{1,2}, Na Li^{1,2}, Hong Li³, Jie Duan³, Bin Li¹, Jigang Li³, Seth J. Davis^{4,5}, and Lei Wang^{1,2,*}

¹Key Laboratory of Plant Molecular Physiology, CAS Center for Excellence in Molecular Plant Sciences, Institute of Botany, Chinese Academy of Sciences, Beijing, 10093, People's Republic of China

²University of Chinese Academy of Sciences

³State Key Laboratory of Plant Physiology and Biochemistry, College of Biological Sciences, China Agricultural University, Beijing 100193, China

⁴University of York, Department of Biology, Heslington, York YO10 5DD, UK

⁵State Key Laboratory of Crop Stress Biology, School of Life Sciences, Henan University, Kaifeng 475004, China

#These authors contributed equally to this study.

Short title: TIC negatively regulates phyA activity

One-sentence summary: TIME FOR COFFEE positively regulates far-red light inhibited hypocotyl growth in *Arabidopsis* by managing the accumulation of the dawn-phased photoreceptor phytochrome A.

The author responsible for distribution of materials integral to the findings presented in this article in accordance with the policy described in the Instructions for Authors (www.plantcell.org) is: Lei Wang (wanglei@ibcas.ac.cn).

ABSTRACT

To enhance plant fitness under natural conditions, the circadian clock is synchronized and entrained by light via photoreceptors. In turn, the circadian clock exquisitely regulates the abundance and activity of photoreceptors via largely uncharacterized mechanisms. Here we show that the clock regulator TIME FOR COFFEE (TIC) controls the activity of the far-red light photoreceptor phytochrome A (phyA) at multiple levels in *Arabidopsis thaliana*. Null mutants of *TIC* displayed dramatically increased sensitivity to light irradiation with respect to hypocotyl growth, especially to far-red light. RNA-sequencing demonstrated that TIC and phyA play largely opposing roles in controlling light-regulated gene expression at dawn. Additionally, TIC physically interacts with the transcriptional repressor TOPLESS (TPL), which was associated with the significantly increased *PHYA* transcript levels in the *tic-2* and *tpl-1* mutants. Moreover, TIC interacts with phyA in the nucleus, thereby affecting phyA protein turnover and the formation of phyA nuclear speckles following light irradiation. Genetically, *phyA* was found to act downstream of *TIC* in regulating far red light-inhibited growth. Taken together, these findings indicate that TIC acts as a major negative regulator of phyA by integrating transcriptional and post-translational mechanisms at multiple levels.

IN A NUTSHELL

Background: To enhance plant adaptability to natural conditions, the circadian clock is synchronized and entrained by light via photoreceptors. Intriguingly, the circadian clock also fine-tunes the abundance and activity of photoreceptors. The photoreceptor phyA accumulates during the night with a peak at dawn, followed by decreasing levels from dawn to dusk, suggesting that the circadian clock plays an indispensable role in regulating phyA accumulation. However, the underlying mechanism is unclear. TIME FOR COFFEE (TIC) was characterized as a clock regulator in *Arabidopsis thaliana* with a peak signaling function prior to dawn and was proposed to modulate light input to the clock at pre-dawn.

Question: We tried to fill in the gaps in our understanding of how the circadian clock exquisitely regulates photoreceptors. We tested whether the clock regulator TIC regulates phyA abundance and activity and unmasked the underlying mechanisms.

Findings: *Arabidopsis tic* mutants exhibit significantly reduced hypocotyl length in a range of continuous far-red fluences, suggesting they are hypersensitive to far-red light. *PHYA* and *FAR-RED-ELONGATED HYPOCOTYLI-LIKE/FAR-RED ELONGATED HYPOCOTYLI*, the key components of the far-red signaling pathway, were upregulated in *tic* mutants at pre-dawn. TIC recruits the transcriptional co-repressor TOPLESS to bind to the *PHYA* promoter to inhibit its pre-dawn transcriptional expression. In addition, TIC physically interacts with phyA in the nucleus to promote its proteolysis following light irradiation. TIC also regulates phyA photobody formation in far-red light. Therefore, the clock component TIC functions as a major negative regulator of phyA by integrating transcriptional and post-translational mechanisms.

Next steps: TIC might function as an emerging cellular hub, integrating environmental information and regulating plant growth. However, the biological function of TIC is still

unclear, and the underlying mechanisms of how TIC coordinates with diverse proteins to regulate plant growth and development need to be further investigated.

1 INTRODUCTION

2 The circadian clock allows plants to adapt to dynamic changes in the external light
3 environment with a ~24 h rhythmic periodicity. This mechanism coordinates plant growth
4 and development within the intrinsic diel and seasonal rhythms in a robust oscillation pattern
5 (Nohales and Kay, 2016; Shalit-Kaneh et al., 2018; McClung, 2019). A complex interplay
6 between the circadian clock and phytochrome photoreceptors has been implicated in plants.
7 The circadian clock regulates the transcription, nuclear import and subsequent intranuclear
8 speckle formation of phytochromes (Toth et al., 2001; Kircher et al., 2002; Wenden et al.,
9 2011; Sanchez et al., 2020). Among the five phytochromes, phytochrome A (phyA) was
10 shown to accumulate during the night and reach its peak at dawn (Sharrock and Clack, 2002).
11 In turn, phyA mediates the perception of far-red (FR) light input to the circadian clock under
12 FR/dark cycles (Wenden et al., 2011). Consistently, *Arabidopsis thaliana phyA* mutants
13 display a lengthened circadian period under low-fluence red or blue light, while *PHYA*
14 overexpression shortens the circadian period in a light-dependent manner (Somers et al.,
15 1998; Kolmos et al., 2011). In addition to its role in regulating circadian-clock periodicity,
16 phyA also coordinates many other clock-driven aspects of plant growth and development,
17 including seed germination, hypocotyl growth during the shade avoidance response,
18 anthocyanin biosynthesis, and flowering time (Casal et al., 2014; Seaton et al., 2018; Yang et
19 al., 2018; Zhang et al., 2018a). Therefore, the close interplay between the clock and phyA

20 signaling is critical for plant response to rhythmic environmental light cues.

21 Unlike the four other light-stable phytochromes in Arabidopsis, phyA is light-labile
22 (Shanklin et al., 1987) and was termed a type I phytochrome (Abe et al., 1985). With this
23 unique feature, phyA protein is detected in an oscillating fashion under diurnal conditions
24 (Sharrock and Clack, 2002). Under photoperiodic conditions, phyA protein has delayed
25 accumulation during the night and reaches peak levels just before dawn. In the early morning,
26 light facilitates the conformation change of phyA from its red-absorbing form (Pr) to its
27 far-red absorbing form (Pfr), which activates a large set of morning-expressed genes (Seaton
28 et al., 2018). Intriguingly, the protein stability of phyA is greatly reduced in its Pfr form
29 (Shanklin et al., 1987; Fankhauser, 2001). The E3-ligase CONSTITUTIVE
30 PHOTOMORPHOGENIC 1 (COP1) contributes to the ubiquitination of both the Pr and Pfr
31 forms of phyA in the presence of sugar (Seo et al., 2004; Debrieux et al., 2013). Less is
32 known about the mechanisms of Pfr-specific turnover of phyA.

33 The oscillating pattern of phyA over the course of a day is collectively determined by its
34 transcriptional and post-translational regulatory mechanisms (Sharrock and Clack, 2002;
35 Seaton et al., 2018). Therefore, the phyA receptor largely functions as a dawn and
36 photoperiod sensor, with a peak of accumulation early in the morning (Seaton et al., 2018).

37 At the transcriptional level, *PHYA* is regulated by PHYTOCHROME INTERACTING
38 FACTOR 4 (PIF4) and PIF5 to achieve its transcription peak late at night (Toth et al., 2001;
39 Sharrock and Clack, 2002; Seaton et al., 2018), which is consistent with subsequent phyA
40 protein accumulation just before dawn under diurnal conditions (Seaton et al., 2018).

41 Interestingly, under 12 h light/12 h dark (LD) conditions, the nuclear import and subsequent

42 accumulation of phyA protein in photobodies dramatically increase just 10 minutes before
43 dawn (Hall et al., 2003; Sanchez et al., 2020). Both phyA transcript and protein abundance
44 are inhibited from dawn to dusk (Sharrock and Clack, 2002; Casal et al., 2014; Seaton et al.,
45 2018), indicating an indispensable role of the circadian clock in repressing phyA
46 accumulation. However, the underlying mechanism of the circadian-controlled phyA profile
47 remains largely unclear.

48 TIME FOR COFFEE (TIC) was initially characterized as a clock regulator with a peak
49 signaling function prior to dawn (Hall et al., 2003). TIC was also shown to participate in
50 many biological processes, such as the maintenance of metabolic homeostasis and the
51 control of root meristem size and jasmonic acid signaling (Shin et al., 2012; Hong et al.,
52 2014; Shin et al., 2017; Sanchez-Villarreal et al., 2018). The biological function of TIC
53 protein has remained elusive, as it has neither known homologs outside plants nor any of the
54 conserved domains that suggest enzymatic activity for its function (Ding et al., 2007).
55 Although TIC was proposed to regulate light input to the circadian clock prior to dawn, the
56 roles of TIC in light signaling and any underlying mechanism remain elusive.

57 Here we report a role for TIC in light signaling by acting as a major negative regulator
58 of phyA abundance at dawn. We show that TIC interacts with TOPLESS (TPL), a
59 transcriptional co-repressor, which correlates with the inhibition of *PHYA* expression at dawn.
60 Moreover, TIC physically interacts with phyA in the nucleus to promote its proteolysis after
61 light reception. Finally, TIC regulates photobody formation by phyA in far-red light.
62 Together, our findings reveal that the clock regulator TIC is a major negative regulator of the
63 photoreceptor phyA that functions by integrating transcriptional and post-translational

64 mechanisms.

65 **RESULTS**

66 **TIC is a negative regulator of light-inhibited hypocotyl growth**

67 TIC was previously identified as a clock regulator that gates light input during the
68 entrainment of the circadian clock (Hall et al., 2003). How TIC participates in light signaling
69 has remained elusive. We therefore systematically investigated the light responsiveness of
70 the *Arabidopsis tic-2* mutant, a null allele generated via a T-DNA insertion (Ding et al.,
71 2007). The hypocotyl length of *tic-2* was only approximately half that of wild-type plants
72 when grown in a range of continuous far-red (FRc) fluences (Figure 1, A and B), suggesting
73 that *tic-2* is hypersensitive to FRc. Moreover, compared to wild type, *tic-2* seedlings
74 displayed fewer but more pronounced shorter hypocotyls when grown under a range of
75 continuous red light (Rc) or continuous blue light (Bc) conditions (Figure 1, C-F). Finally,
76 *tic-2* seedlings displayed modestly shorter hypocotyls when grown under short day (SD)
77 conditions (Supplemental Figure S1, A and B), but their hypocotyls were comparable to the
78 wild type in continuous darkness (Supplemental Figure S1, C and D). These observations
79 indicate that TIC is a critical regulator of light signaling during hypocotyl growth.

80 To further confirm the role of *TIC* in light signaling, we conducted genome editing to
81 target the first exon of *TIC* using a previously described CRISPR/Cas9 approach (Ma et al.,
82 2015) to generate a null mutation for further phenotypic characterization. We selected a
83 homozygous mutant from T3 progeny. Sanger sequencing confirmed that the genome-edited
84 *tic* mutant contained a 1 bp deletion in the first exon (Supplemental Figure S2, A), which

85 resulted in frame shift and introduction of a premature stop codon encoding only the first 46
86 amino acids. This new allele (hereafter named *tic-3*) displayed the serrated leaves and late
87 flowering under long-day conditions observed in *tic-2* (Supplemental Figure S2B). As
88 expected, *tic-3* also displayed a short circadian period (Supplemental Figure S2, C-F),
89 similar to *tic-2*. We separately tested the light responsiveness of this mutant to FRc, Rc, and
90 Bc. *tic-3* displayed dramatically increased sensitivity to FR but modestly elevated sensitivity
91 to Rc and Bc (Supplemental Figure S3), as observed in *tic-2* (Figure 1). Moreover, when
92 grown under SD conditions, *tic-3* also displayed a short hypocotyl phenotype, but not in
93 continuous darkness (Supplemental Figure S4). Overall, *tic-3* displayed similar phenotypes
94 to *tic-2* in the regulation of light responsiveness, flowering time, and circadian period,
95 suggesting that *tic-2* and *tic-3* are indistinguishable null alleles that can be used
96 interchangeably.

97 To test the genetic complementation of the *tic-2* mutant, we generated a construct
98 harboring *GFP* fused to the *TIC* open reading frame driven by its native promoter (-2,691 bp
99 upstream of the start codon) (*TICpro:GFP-TIC*) and transformed into *tic-2* for genetic
100 complementation analysis. As expected, *TICpro:GFP-TIC* largely rescued the defective
101 response of *tic-2* mutant to light, especially to FRc (Supplemental Figure S5), indicating that
102 the *GFP-TIC* lines could be used for further analysis.

103 **TIC regulates a subset of genes in an opposite manner to phyA at pre-dawn**

104 To further investigate the temporal-specific effects of *TIC*, we conducted
105 RNA-sequencing with tissues harvested at pre-dawn (10 minutes before the lights were
106 turned on) and post-dusk (10 minutes after the lights were turned off) (Supplemental Figure

107 [S6, A](#)). We collected ten-day-old *tic-2* and wild type (Col-0) seedlings grown under LD
108 conditions at pre-dawn and post-dusk, respectively. After strictly screening with a cut-off at
109 fold change > 2, we identified 785 and 567 upregulated differentially expressed genes
110 (DEGs) at ZT0 and ZT12, respectively, and 520 and 237 downregulated DEGs, respectively
111 ([Figure 2, A and B and Supplemental Data Set S1](#)). The repeatability among the biological
112 replicates was confirmed by the high value Pearson correlation coefficient (> 0.98, within
113 biological repeats, [Supplemental Figure S6, B](#)). In addition, heat-map visualization of these
114 DEGs revealed that the scaled expression of the DEGs was highly reproducible among the
115 three biological repeats ([Supplemental Figure S6, C and D](#)).

116 Gene ontology (GO) analysis of the genes with increased expression in *tic-2*
117 demonstrated that the terms circadian rhythm, response to light stimulus, and response to red
118 or far red light were highly enriched both pre-dawn and post-dusk ([Supplemental Figure S7,](#)
119 [A and B](#)). Consistent with the notion that TIC functions as a clock regulator, interaction
120 network analysis with the STRING database revealed that clock-related genes formed a
121 major cluster, including the day-time clock genes *PSEUDO-RESPONSE REGULATOR7*
122 (*PRR7*), *PRR9*, and *LATE ELONGATED HYPOCOTYL (LHY)*, within the 402 overlapping
123 DEGs between pre-dawn and post-dusk ([Supplemental Figure S8](#)). By contrast, GO analysis
124 of downregulated DEGs failed to identify the circadian rhythm cluster at either time point,
125 supporting the notion that TIC functions as a clock regulator, likely by mediating
126 transcriptional repression. Terms related to light signaling were also enriched in the
127 downregulated DEGs pre-dawn, but not post-dusk ([Supplemental Figure S7, C and D](#)),
128 indicating that TIC has a profound effect on regulating light signaling, predominantly during

129 pre-dawn.

130 Given that phyA is the only far-red light photoreceptor identified in Arabidopsis and
131 that it also functions in red light- and blue light-mediated hypocotyl growth, we reasoned
132 that TIC may be involved in regulating phyA-mediated light signaling. Hence, we compared
133 our RNA-Seq data with previously identified direct targets of phyA (Chen et al., 2014). Over
134 26% (44/169) of phyA-repressed genes were markedly upregulated in *tic-2* at pre-dawn,
135 including *PHYTOCHROME RAPIDLY REGULATED1 (PAR1)*, *FAR-RED-ELONGATED*
136 *HYPOCOTYL 1-LIKE (FHL)*, and *FAR-RED ELONGATED HYPOCOTYL 1 (FHY1)* (Figure
137 2, C and D), and 14% (38/265) of phyA-activated genes were downregulated in *tic-2* at
138 pre-dawn (Figure 2, C). By contrast, only 4% (7/169) of phyA-repressed genes and less than
139 2% (5/265) of phyA-activated genes overlapped with the DEGs identified in *tic-2* post-dusk
140 (Supplemental Figure S9), suggesting that TIC regulates a subset of genes in an opposite
141 manner to phyA, predominantly at pre-dawn. This was further substantiated by time course
142 qRT-PCR (Figure 2, E-G and Supplemental Figure S10). Consistently, *FHL*, *PAR1*, and *PIL1*
143 also displayed a similar time-course expression pattern in *tic-3* (Supplemental Figure S11).
144 Together, we conclude that a subset of genes, including those encoding FR signaling
145 components, are regulated in an opposite manner by TIC and phyA in a time-of-day specific
146 manner, mainly at dawn.

147 **TIC likely represses *PHYA* transcription by associating with its promoter**

148 Our RNA-seq data also showed that *PHYA* was significantly upregulated in *tic-2* at
149 pre-dawn, which is consistent with previous microarray data (Sanchez-Villarreal et al., 2013)
150 (Supplemental Data Set S1). This was further verified by time course qRT-PCR, in which

151 *PHYA* transcript levels increased in the *tic-2* and *tic-3* mutants at dawn (Figure 3, A,
152 Supplemental Figure S11A). We also examined the transcript level of *PHYA* in *tic-2* under
153 constant light conditions and found that it was higher at subjective dawn but not at subjective
154 night (Supplemental Figure S12). Since our RNA-seq analysis suggested that TIC plays a
155 pervasive role in transcriptional repression, together with the higher transcript levels of
156 *PHYA* and other FR signaling components (such as *FHY1* and *FHL*) in *tic-2*, we investigated
157 whether TIC could repress their transcription *in planta* using a transient expression assay in
158 *Nicotiana benthamiana* leaves. The expression of GFP-TIC dramatically repressed the
159 promoter activity of *PHYA* relative to the *GFP* controls (Figure 3, B-D). These results
160 suggest that TIC transcriptionally represses *PHYA* expression.

161 We next examined if TIC could directly associate with *PHYA* promoter by performing
162 a chromatin immunoprecipitation (ChIP) assay with the *TICpro:GFP-TIC tic-2* line
163 (Supplemental Figure S5). The plants were grown under LD photocycles, and samples were
164 harvested at ZT0 (zeitgeber time 0) when the *PHYA* transcript level was highest in *tic-2*
165 (Figure 3, A), and at ZT12 when the *PHYA* transcript was as low as the control. Our
166 ChIP-qPCR assay demonstrated that among the nine tested amplicons (Figure 3, E, upper
167 panel), amplicon S5 was modestly but significantly enriched with *GFP-TIC* relative to *GFP*
168 alone at ZT0, but not at ZT12 (Figure 3, E, lower panel, Supplemental Figure S13). However,
169 no significant enrichment of the amplicon corresponding to the housekeeping gene *APX3*, a
170 negative control, was detected. In addition, another core clock component, GFP-TOC1,
171 failed to effectively bind to the *PHYA* promoter (Supplemental Figure S14), further
172 indicating that the binding of GFP-TIC to the *PHYA* promoter was not due to its GFP tag.

173 Together, these data suggest that TIC associates with the *PHYA* promoter in a region close to
174 the transcription start site (TSS).

175 Consistent with the notion that TIC protein associates with the *PHYA* promoter to
176 repress its transcription, *PHYA* transcript levels were higher in *tic-2* vs. Col-0 in constant
177 darkness and decreased after transfer to red light (R) for 60 min (Figure 3, F, Supplemental
178 Figure S15). Consistently, phyA protein levels were also higher in *tic-2* either in constant
179 darkness (DD) or after transfer to R, which can facilitate its protein degradation (Figure 3,
180 G). In addition, we generated separate truncated versions of *PHYA* promoters with deletion
181 of region S4, S5, or S6 to drive the luciferase gene. TIC still successfully inhibited their
182 expression (Supplemental Figure S16), suggesting that TIC inhibits *PHYA* promoter activity
183 via an alternate mechanism. Taken together, our data suggest that TIC is involved in
184 repressing *PHYA* transcription, possibly via direct or indirect mechanisms.

185 **TIC interacts with TPL in the nucleus**

186 To gain further insight into the role of TIC in transcriptional regulation and
187 phyA-mediated FR signaling, we searched for its nuclear interactome by performing
188 affinity purification-mass spectrometry (AP-MS) (Wang et al., 2020). Entrained
189 *TICpro:GFP-TIC tic-2* transgenic seedlings under LD conditions were collected at pre-dawn,
190 when TIC regulates light input to the circadian clock and *PHYA* transcript level (Hall et al.,
191 2003). In total, we identified 43 nuclear proteins immunoprecipitated by GFP-TIC among
192 three biological replicates. These included phyA, TOPLESS (TPL), CHROMATIN
193 REMODELING 4/19 (CHR4/19), and SSRP1 (SSRP1), a subunit of the FACT (facilitates
194 chromatin transcription) complex (Figure 4, A and Supplemental Data Set S2).

195 TPL was previously characterized as a transcriptional co-repressor that interacts with
196 EAR (ethylene-responsive element binding factor-associated amphiphilic repression) motif
197 (LxLxL)-containing proteins (Pauwels et al., 2010; Wang et al., 2013; Ito et al., 2016;
198 Martin-Arevalillo et al., 2017). Visual inspection of the amino acid sequence of TIC led us to
199 detect a motif resembling an EAR motif from its 566th to 571st amino acid residues
200 (LKLDLD). As our RNA-seq data suggested that TIC likely functions in repressing
201 transcription, and because the co-repressor TPL is a potential interacting protein of TIC
202 (Figure 4, B), we substantiated the physical interaction between TPL and TIC proteins.
203 Using transient coexpression of TPL-FLAG and GFP-TIC in *N. benthamiana* leaves, we
204 detected the coimmunoprecipitation of TPL-FLAG with GFP-TIC, but not with the GFP
205 control (Figure 4, C). Moreover, the interaction between TIC and TPL was drastically
206 weakened by the point mutation of the proposed EAR domain of TIC (Supplemental Figure
207 S17).

208 As nuclear presence is a prerequisite for TPL acting as a transcriptional co-repressor of
209 TIC, we performed a biofluorescence complementation (BiFC) assay in *N. benthamiana*
210 leaves to examine the subcellular localization and the *in planta* interactions between TIC and
211 TPL. As expected, we found a strong nuclear YFP (yellow fluorescence protein) signal when
212 TPL-nYFP was coexpressed with TIC-cYFP (Figure 4, D). In addition, the transcript level of
213 *PHYA* in *tpl-1*, a dominant negative mutant of *TPL* (Long et al., 2006), was significantly
214 higher at ZT0 but not at ZT12, which is consistent with the notion that TPL acts as a
215 co-repressor of TIC to repress *PHYA* transcription at dawn (Figure 4, E). Consistently, TPL
216 also bound to the S5 region of the *PHYA* promoter in the presence of TIC (Supplemental

217 [Figure S18](#)). Neither TIC with the EAR point mutation nor co-expression with TPL
218 significantly affected the repressive effect of TIC on *PHYA* promoter activity ([Supplemental](#)
219 [Figure S19](#)), further indicating that TIC employs an alternative mechanism to repress *PHYA*
220 expression.

221 The *tpl-1* mutant displayed modestly shorter hypocotyl than Col-0 grown under FRc,
222 similar to *tic* mutants ([Figure 4, F and G](#)). The less pronounced hypocotyl phenotype of *tpl-1*
223 in FRc may be due to the interaction of TPL with other transcriptional regulators that have
224 antagonistic interactions with TIC to regulate hypocotyl growth or perhaps to the functional
225 redundancy of its family members. Indeed, TPL is a co-repressor of IAA repressor proteins
226 and the clock components PRRs (Long et al., 2006; Wang et al., 2013), and the compromised
227 repressor activity of IAA and PRR in *tpl-1* diminishes their inhibition of PIF4/5 and auxin
228 signaling to promote hypocotyl growth (Long et al., 2006; Wang et al., 2013; Zhu et al.,
229 2016; Li et al., 2020). These findings support the notion that TIC acts as a transcription
230 regulator by interacting with TPL to repress downstream genes such as *PHYA*, thereby
231 regulating hypocotyl growth in FRc.

232 **TIC physically interacts with phyA**

233 To verify our AP-MS data showing the TIC-phyA interaction *in vivo* ([Figure 5, A](#)), we
234 co-expressed *GFP-TIC* and *PHYA-HA* in *N. benthamiana* leaves and measured binding via a
235 co-immunoprecipitation assay. Consistent with our AP-MS result, we observed a positive
236 interaction of GFP-TIC with PHYA-HA ([Figure 5, B, upper panel](#)), but not with PHYB-HA
237 ([Figure 5, B, lower panel](#)). Since phyA protein can localize to both the cytosol and the

238 nucleus, to determine where the interaction between TIC and PHYA occurs, we performed a
239 BiFC assay by co-infiltrating *TIC-nYFP* and *PHYA-cYFP* into *N. benthamiana* leaf
240 epidermal cells. As shown in [Figure 5 C](#), we observed a reconstituted YFP signal in the
241 nucleus in the presence of both TIC-nYFP and PHYA-cYFP, supporting the notion that TIC
242 and phyA interact in the nucleus.

243 We then used the LexA yeast two-hybrid system to determine the regions mediating the
244 TIC and PHYA interaction (Zhang et al., 2018a). The histidine kinase-related domain
245 (designated as C2) of phyA fused with the LexA DNA binding domain displayed a stronger
246 interaction with the C-terminus of TIC (755-1555 aa) than with its N-terminus (1-744 aa)
247 ([Figure 5, D](#)), indicating that phyA and TIC interacted in yeast cells. Finally, we conducted a
248 co-immunoprecipitation assay by co-expressing *TIC-NT-GFP* or *TIC-CT-GFP* with
249 *PHYA-HA* in *N. benthamiana*. Consistently, we observed a strong interaction between
250 TIC-CT-GFP and PHYA-HA, while there was a much weaker interaction between
251 TIC-NT-GFP and PHYA-HA, suggesting that TIC-CT functions directly in mediating its
252 interaction with phyA ([Figure 5, E](#)). Taken together, these results indicate that TIC interacts
253 with phyA in the nucleus.

254 **TIC negatively regulates phyA protein abundance**

255 As phyA and TIC proteins physically interact with each other, we tested if phyA is
256 regulated by TIC at a post-transcriptional level. First, we explored whether TIC is involved
257 in regulating phyA protein stability. To eliminate the effect of TIC on *PHYA* transcription,
258 *PHYA-LUC* driven by the CaMV 35S constitutive promoter was co-infiltrated with *GFP-TIC*
259 or *GFP* control into *N. benthamiana* leaves. The bioluminescence signal of PHYA-LUC

260 decreased by 60% in the presence of GFP-TIC relative to the GFP control (Figure 6, A).
261 Consistently, immunoblotting with anti-LUC antibody revealed a similar reduction in
262 PHYA-LUC protein abundance by GFP-TIC (Figure 6, B), suggesting that phyA protein
263 accumulation is diminished by the presence of GFP-TIC.

264 As TIC is also involved in repressing *PHYA* transcription, to further corroborate if the
265 turnover of phyA is facilitated by TIC and to eliminate the effect of transcriptional inhibition
266 of TIC on *PHYA*, we introgressed the previously generated *35S:PHYA-YFP* (Yang et al.,
267 2018) into the *tic-2* mutant background by genetic crossing. As phyA was most abundant in
268 dark-grown seedlings but was rapidly depleted after light treatment (Sharrock and Clack,
269 2002), we first examined the degradation rate of phyA protein by separately transferring
270 etiolated *35S:PHYA-YFP* and *35S:PHYA-YFP tic-2* seedlings to FR or R at specific times.
271 Consistent with the previous finding that phyA protein was rapidly degraded in R,
272 PHYA-YFP degraded much more rapidly under R compared to FR (Figure 6, C-F). The
273 rates of PHYA-YFP degradation under both R and FR were markedly reduced in *tic-2*
274 (Figure 6, C-F). We then assessed the turnover of PHYA-YFP in the presence of TIC under
275 diurnal conditions. PHYA-YFP protein abundance during the daytime was higher in *tic-2* vs.
276 Col-0 in both the presence (Figure 6, G and H) and absence of sucrose (Supplemental Figure
277 S20), further suggesting that TIC facilitates PHYA-YFP protein degradation in a
278 light-dependent manner that is not dependent on exogenous sucrose addition.

279 As phyA can aggregate into speckles in response to light exposure (Kircher et al., 1999;
280 Nagatani, 2004), we next tested if the formation of these phyA photobodies was altered in
281 the *tic-2* mutant. To this end, we examined fluorescent PHYA-YFP signals in etiolated

282 seedlings after a range of light exposures. As expected, we detected increased PHYA-YFP
283 signals in the nucleus and increased photobody formation in response either FR or R. These
284 effects were markedly higher in *tic-2* than the wild type (Supplemental Figure S21). This
285 was not due to increased phyA accumulation, as both total and nuclear PHYA-YFP protein
286 levels were comparable between *tic-2* and Col-0 after a short light exposure (Supplemental
287 Figure S22). Hence, we conclude that not only the protein turnover of phyA, but also its
288 formation of photobodies, were affected by TIC.

289 **phyA is epistatic to TIC in mediating FR-repressed hypocotyl elongation**

290 Our findings demonstrate that TIC negatively regulates phyA abundance by both
291 repressing its transcription and facilitating its proteolysis. Therefore, we reasoned that the
292 shorter hypocotyls of *tic-2* under FRc are predominantly caused by abnormally high levels of
293 phyA accumulation. To genetically test this hypothesis, we examined the hypocotyl growth
294 of *tic-2*, *phyA-211*, and *tic-2 phyA-211* in response to FRc, Rc, and Bc. Consistent with a
295 previous report, *phyA-211* seedlings displayed longer hypocotyls when grown under a range
296 of FRc fluences, while *tic-2* seedlings had shorter hypocotyls. *tic-2 phyA-211* displayed
297 markedly longer hypocotyls than Col-0 (Figure 7, A and B). In most cases, the hypocotyl
298 length of *tic-2 phyA-211* was comparable to that of the *phyA-211* single mutant under the
299 FRc fluences examined, supporting the notion that *phyA-211* is genetically epistatic to *tic-2*
300 in response to FR.

301 The shorter hypocotyls of *tic-2* grown under low-intensity Bc were largely rescued by
302 the introgression of *phyA-211*, but not under the Rc fluence examined (Figure 7, C-F),
303 further supporting the notion that phyA is genetically required for the effect of TIC on

304 hypocotyl growth under FRc and low Bc light conditions. Nonetheless, we noticed that the
305 hypocotyls of the *tic-2 phyA-211* double mutant grown under Rc and high Bc light
306 conditions were still slightly shorter than those of *phyA-211* (Figure 7, C-F), suggesting that
307 other downstream targets of TIC might also mediate the inhibitory effect of TIC on
308 hypocotyl growth.

309 Finally, we examined the transcript levels of FR signaling components in via
310 time-course qRT-PCR. The transcript levels of the genes that were regulated in an opposite
311 manner by *phyA* and TIC, including *FHY1*, *FHL*, *PAR1*, *PIL1*, and *HB2*, were still much
312 higher in the *tic-2 phyA-211* double mutant than the wild type at dawn (Figure 8, A-E). These
313 results suggest that the effect of transcriptional inhibition of these genes by TIC is not fully
314 dependent on *phyA* protein levels, which may collectively contribute to enhanced FR
315 signaling in *tic* mutants. The short hypocotyls of *tic-2* grown under SD could not be rescued
316 by *phyA-211* (Supplemental Figure S23), indicating that other downstream components of
317 TIC are involved in this process. Taken together, we conclude that *PHYA* is a major
318 downstream target of TIC that mediates its regulation of FR signaling, while other
319 downstream targets (including FR signaling and clock components) act in concert with *phyA*
320 to mediate the comprehensive effects of TIC on light responsiveness (Figure 9).

321 **DISCUSSION**

322 The abundance and activity of *phyA* are under tight circadian control, but the
323 underlying mechanisms are largely uncharacterized. Here we demonstrated that TIC, a clock
324 regulator lacking conserved domains with unclear biochemical functions, plays multiple
325 inhibitory roles in repressing *phyA* signaling at both the transcriptional and post-translational

326 levels. Our findings suggest that one biological role of TIC is to function as a member of the
327 transcriptional repressive complex by associating with the transcriptional co-repressor TPL
328 (Figure 9). Intriguingly, TIC also modulates protein stability via direct physical interactions
329 with its targets, such as MYC2 (Shin et al., 2012) and phyA (Figure 6). Our findings show
330 that TIC protein is a major negative regulator of phyA that regulates its transcription and
331 protein stability, perhaps representing an important molecular link of clock-profiled phyA
332 signaling.

333 Interestingly, the transcript levels of *FHY1* and *FHL*, encoding proteins required for
334 the transport of the Pfr form of phyA into the nucleus, were also significantly higher in *tic-2*
335 than the wild type, suggesting that TIC might repress phyA signaling at multiple entry points
336 (Figure 2, F and G) besides directly regulating phyA abundance. However, it seems that
337 phyA is not required for the inhibition of a subset of genes including *FHY1* and *FHL* by TIC,
338 as their transcript levels were much higher in the *tic-2 phyA-211* double mutant than the wild
339 type, especially at pre-dawn. Hence, it is conceivable that TIC simultaneously regulates a
340 few core components to attenuate phyA-mediated light signaling at the transcriptional level
341 in a time-of-day specific manner (Figure 9).

342 Under photoperiodic conditions, phyA protein accumulates during the night and is
343 rapidly degraded during the day upon exposure to light (Sharrock and Clack, 2002). By
344 contrast, the number of nuclear speckles containing phyA is higher in the daytime than at
345 night (Kircher et al., 2002), indicating that the regulation of phyA abundance and
346 localization are subject to circadian control. Here we showed that TIC strongly regulates
347 phyA abundance at pre-dawn but not at post-dusk (Figure 3). In addition, the intensity of

348 phyA photobody formation upon FR or R irradiation was significantly higher in the *tic-2*
349 mutant than Col-0, which is consistent with its elevated phyA signaling in connection to
350 hypocotyl growth (Figure 1).

351 COP1 was previously proposed to be a E3 ubiquitinase of phyA apoprotein that
352 facilitates its protein degradation via the 26S proteasome pathway (Seo et al., 2004).
353 However, as the *cop1-4* and *cop1-6* mutants only displayed modestly reduced rates of phyA
354 degradation, additional pathways are thought to be required for phyA degradation. In this
355 study, COP1 protein levels were even higher in *tic-2* seedlings than Col-0 when grown under
356 continuous R or FR light, which further suggests that the promotion of phyA protein
357 turnover by TIC is likely independent of COP1 (Supplemental Figure S24). Hence, the role
358 of TIC in regulating phyA might represent a link between circadian clock-regulated phyA
359 abundance and localization. Notably, under light irradiation conditions, COP1 gradually
360 relocates from the nucleus to the cytosol (von Arnim and Deng, 1994; von Arnim et al.,
361 1997). TIC is predominantly located to the nucleus and thus may act as a positive regulator
362 of phyA degradation in the nucleus, which may determine the light labile properties of phyA
363 apoprotein. It will be fascinating to clarify the biochemical function of TIC in destabilizing
364 its interacting targets.

365 Intriguingly, it was previously demonstrated that TIC interacts with MYC2 to affect its
366 protein abundance specifically at dusk (Shin et al., 2012). The difference in the timing of
367 TIC-regulated phyA vs. MYC2 abundance could be due to differences in the availability of
368 their respective E3 ubiquitin ligases, which should be fully addressed in the future.

369 When grown under SD conditions, the hypocotyl length of the *tic-2 phyA-211* double

370 mutant was equivalent to that of the *tic-2* single mutant, indicating that phyA itself is not
371 sufficient to mediate TIC-regulated hypocotyl growth under photoperiodic conditions.
372 Consistently, the hypocotyl length of SD-grown *phyA-211* was not significantly different
373 from the wild type. Given that TIC also functions as a clock regulator, and clock genes
374 including *TOC1* and *ELF3* displayed the altered expression patterns in the *tic* mutant
375 (Supplemental Figure S7) (Ding et al., 2007), it is conceivable that multiple clock
376 components mediate the regulation of hypocotyl growth by TIC, either directly or indirectly.
377 Together, we propose that TIC regulates multiple genes at the transcriptional level, in concert
378 with its role in regulating phyA protein stability, which together coordinate hypocotyl growth
379 in response to light signals.

380 Approximately one-fifth of all transcription factor genes identified to date display
381 differential expression patterns in *tic-2* (Shin et al., 2012). Here we found that TIC associated
382 with the *PHYA* promoter to regulate its transcription (Figure 3), suggesting that TIC may
383 function as a general transcriptional regulator that modulates the abundance of numerous
384 transcription factors (either directly or indirectly) to form a complex transcriptional cascade
385 network that modulates multiple physiological processes. As the expression of *TIC* itself
386 does not oscillate robustly, its dawn-phased transcriptional activity is likely determined by an
387 uncharacterized transcription factor whose levels peak at dawn. Intriguingly, phyA directly
388 targets numerous promoters to directly mediate multiple biological processes (Chen et al.,
389 2014). Here we showed that TIC inhibits the accumulation of phyA at both the
390 transcriptional and post-translational levels. Perhaps their physical interaction affects the
391 function of TIC, and vice versa, on target gene transcription.

392 phyA is thought to regulate gene expression via an escort model in which it controls
393 the availability of transcription factors, or via a proxy model in which it regulates gene
394 expression by physically associating with transcription factors (Chen et al., 2014). A similar
395 situation was observed for the blue-light photoreceptor CRY2, which interacts with a few
396 transcriptional regulators to repress their activities (Liu et al., 2008). It will be of great
397 interest to decipher the role of phyA in regulating TIC activity, especially whether the
398 regulatory roles of phyA on TIC represents a light input pathway to the clock.

399 Given that TIC has been shown to regulate the circadian clock, modulate metabolic
400 homeostasis, affect phytohormone biosynthesis, and function in the signaling pathways of
401 phytohormones including auxin, jasmonate, and abscisic acid, it will be fascinating to further
402 investigate the balance or tradeoff of these downstream events mediated by TIC. One
403 possible way is through interacting with distinct proteins that are crucial components of the
404 respective pathways. Our finding that TIC participates in phyA- and core clock
405 component-mediated hypocotyl growth further reinforces the notion that TIC functions as an
406 emerging cellular hub that integrates environmental information to regulate plant growth to
407 achieve better plant fitness in an ever-changing environment, likely (in part) through phyA
408 signaling. This, in turn, could have wide-ranging roles in multiple growth-control processes,
409 such as brassinosteroid, auxin, abscisic acid, and various stress signaling pathways. Future
410 efforts to decipher the networks and understand the tradeoffs among different downstream
411 events may provide a basis for molecular design breeding of crops.

412 **MATERIAL AND METHODS**

413 **Plant Materials and Growth Conditions**

414 The Columbia (Col-0) ecotype of *Arabidopsis thaliana* was used in this study. The
415 *tic-2*, *phyA-211*, and *tpl-1* mutants and the *35S:PHYA-YFP* transgenic line in the Col-0
416 background were described previously (Ding et al., 2007; Yang et al., 2018; Zhang et al.,
417 2018a). The *tic-2 phyA-211* double mutant was generated by crossing *tic-2* to *phyA-211* and
418 confirmed genotypically. All primers used for mutant genotyping are listed in Supplemental
419 Table S1. To generate the *tic-3* mutant, the CRISPR/Cas9-mediated genome-editing system
420 was used in Col-0 background (see below for vector construction).

421 The growth conditions were 12-h light/12-h dark, white light ($200 \mu\text{mol m}^{-2} \text{s}^{-1}$), 22 °C
422 (LD); constant darkness, 22 °C (DD); or constant white light (Light Emitting Diode, 200
423 $\mu\text{mol m}^{-2} \text{s}^{-1}$), 22 °C (LL), as noted. For hypocotyl length assays, seeds were surface
424 sterilized and grown on half strength of Murashige and Skoog (MS) medium containing 1%
425 sucrose, stratified for 3 days, and exposed to white light ($200 \mu\text{mol m}^{-2} \text{s}^{-1}$) for 7-9 h to
426 induce germination before being transferred to a light chamber under ~ 0.1 , 0.3, 0.5, and 1
427 $\mu\text{mol m}^{-2} \text{s}^{-1}$ far red light (FR), ~ 5 , 10, 20, and 40 $\mu\text{mol m}^{-2} \text{s}^{-1}$ red light (R), or 1, 5, 10, and
428 20 $\mu\text{mol m}^{-2} \text{s}^{-1}$ blue light (B). Hypocotyl length was calculated for 5-day-old seedlings that
429 were photographed (Canon) and measured using NIH ImageJ software
430 (<http://rsbweb.nih.gov/ij/>). To examine circadian phenotypes, surface sterilized seeds were
431 grown under LD conditions on MS containing 3% sucrose for 8 days and transferred to
432 constant red or blue light ($40 \mu\text{mol m}^{-2} \text{s}^{-1}$), as indicated. For the affinity purification assay
433 followed by mass spectrometry, two-week-old seedlings grown under LD conditions were
434 harvested at pre-dawn (10 min before lights on).

435 **Vector Construction and Plant Transformation**

436 To produce *TICpro:GFP-TIC tic-2* transgenic plants, the fragment of *TIC* promoter
437 (-2691 to -1 bp, upstream of the start codon) was amplified and inserted into *Pst* I and *Kpn* I
438 sites of the *p1300* promoter-less vector (Wang et al., 2013), followed by subcloning
439 *GFP-TIC* through the *Kpn* I and *Nco* I sites, and transformed into *Agrobacterium* by the
440 floral dip method (Clough and Bent, 1998). To generate *35S:GFP-TIC-NT* and
441 *35S:GFP-TIC-CT*, the respective PCR fragments were subcloned into the *Kpn* I and *Xho* I
442 sites of the *pENTR2B* vector and subcloned into the *35S:GFP-MDC45* vector via LR
443 reaction. To generate the *pCsVMV:PHYA-HA* construct, the fragment was amplified by PCR
444 and subcloned into the *Kpn* I and *Bam*H I sites of the *pCsVMV:HA-1300* vector (Wang et al.,
445 2013).

446 To generate *PHYApro:LUC* (-1932 to -1 bp, upstream of the start codon), the promoter
447 was amplified from Col-0 genomic DNA and inserted into the promoter-free *pLUC-N-1300*
448 vector between the *Pst* I and *Kpn* I sites. To produce the *CsVMV:PHYA-LUC* construct, the
449 coding sequence of *LUC* fragment was amplified by PCR and subcloned into the *Xma* I and
450 *Nco* I sites of the *pCsVMV:HA-1300* vector. The *PHYA* fragment was amplified by PCR and
451 subcloned into *Kpn* I and *Xma* I sites of *pCsVMV:LUC-1300* vector.

452 To generate constructs for the yeast two-hybrid assay, the *TIC*, *TIC-NT*, and *TIC-CT*
453 fragments were amplified by PCR and inserted into the pB42AD vector via *Eco*R I and *Xho*
454 I sites to generate the *AD-TIC*, *AD-TIC-NT*, *AD-TIC-CT* constructs, respectively. The
455 *LexA-PHYA-N*, *LexA-PHYA-C1*, *LexA-PHYA-C2* constructs were used as previously
456 described (Zhang et al., 2018a).

457 The *tic-3* mutant was generated by CRISPR (Clustered Regularly Interspaced Short
458 Palindromic Repeats)/Cas9-mediated gene editing as a previously described (Ma et al.,
459 2015). Briefly, the sgRNA (single-guide RNA, as listed in Supplemental Table S1) was
460 designed to target the first exon of *TIC*. The sgRNA was cloned into the
461 *pYLCRISPR/Cas9Pubi-MH* vector (Ma et al., 2015). The resulting construct was
462 transformed into *Agrobacterium tumefaciens* to obtain gene-edited Arabidopsis lines by the
463 floral dip method (Clough and Bent, 1998).

464 **Total RNA extraction and qRT-PCR**

465 Total RNA was extracted from ten-day-old Arabidopsis seedlings using the TRIzol
466 reagent (Invitrogen, Carlsbad, CA, USA) according to the manufacturer's protocol and
467 treated with RNase-free DNase I (Thermo Fisher) before reverse transcription. Seedlings
468 were grown on MS medium under LD or LL conditions and harvested over a time course, as
469 noted. First-strand cDNA was synthesized using tM-MLV reverse transcriptase (Promega)
470 and oligo-dT primers. qRT-PCR was performed using SYBR Green Real-Time PCR Master
471 Mix (Toyobo, Osaka, Japan) according to the manufacturer's instructions on an Applied
472 Biosystems QuantStudio 3 instrument (Applied Biosystems, Thermo Fisher Inc.). *ACTIN2*
473 (*AT3G18780*) and *PP2A* (*AT1G69960*) were used for normalization. The mRNA expression
474 levels were calculated by the $2^{-\Delta C(t)}$ method from three biological replicates (separate
475 experiments) and three technical replicates (identical samples within an experiment) as
476 described previously (Wang et al., 2013). The RT-qPCR primers for the respective genes in
477 this study are listed in Supplemental Table S1.

478 **RNA-Sequencing and data analysis**

479 For RNA-Sequencing, Col-0 and *tic-2* seedlings were grown on MS with 3% sucrose
480 under LD conditions for 10 days and then collected at pre-dawn (10 min before lights on)
481 and post-dusk (10 min after light off). Library generation and sequencing were performed as
482 previously described by Annoroad Gene Technology (Beijing, China) (Zhang et al., 2018b).
483 In brief, RNA-seq clean reads were mapped to the reference genome with HISAT2 (v2.1.0,
484 Sirén et al. 2014) after filtering out low-quality reads. Genes with expression levels of
485 FPKM (fragments per kilobase of exon model per million reads mapped) > 0.1 were
486 considered to be expressed and used for further analysis (Trapnell et al., 2010). Uniquely
487 aligned reads were counted for each annotated gene using the program HTSeq (v0.6.0).
488 Differential gene expression was evaluated using the DESeq2 (v1.6.3) to determine fold
489 change and q value, which is an adjusted p value to account for multiple testing; DEGs with
490 $|\log_2 \text{Fold change}| \geq 1$ and $q < 0.05$ were determined to be differentially expressed. The
491 fisher.test and p.adjust were used for GO (gene ontology) enrichment analysis and KEGG
492 (Kyoto Encyclopedia of Genes and Genomes) analysis. The Integrative Genomics Viewer
493 was used to visualize the reads for selected genes (Robinson et al., 2011; Thorvaldsdottir et
494 al., 2013).

495 **Affinity Purification Followed by Mass Spectrometry**

496 Two-week-old *TICpro:GFP-TIC* and *35Spro:GFP* seedlings were harvested at
497 pre-dawn and quickly frozen in liquid nitrogen. Affinity purification followed by mass
498 spectrometry was performed as previously described (Wang et al., 2020). Briefly, 3 mL of
499 ground tissue for each sample was used for protein extraction with 3 mL protein extraction

500 buffer. After homogenization, the clear supernatant was incubated with GFP-Trap beads
501 (ChromoTek) for 1 h at 4 °C with rotation. The beads were washed in ice-cold washing
502 buffer I; this step was repeated four times, followed by three rinses with washing buffer II.
503 An iST Sample Preparation kit (P.O.00027, PreOmics, Germany) was used for the next step.
504 After purification, the samples were separated into two equal parts and individually used for
505 spectral library building and quantitation analysis via the SWATH method. LC-MS was
506 performed at an on-site facility with an OrbiTRAP Fusion Lumos mass spectrometer
507 (Thermo Fisher Scientific, USA). All of the data were acquired with SWATH™ Acquisition
508 MicroApp 2.0. For statistical analysis using Student's *t*-test, quantitative data of the peptides
509 were exported to MarkerView software (SCIEX Ltd.). The putative interacting proteins of
510 TIC were identified based on the following criteria: proteins with at least two peptides that
511 were present in both samples of *TICpro:GFP-TIC*, and their abundance compared to the GFP
512 negative control was > 1.5 fold.

513 **Chromatin immunoprecipitation**

514 The ChIP assay was conducted as previously described with slight modifications (Wang et
515 al., 2013). Two-week-old seedlings, grown at 22 °C on MS medium containing 3% sucrose
516 and 0.8% agar under 12 L/ 12 D conditions, were harvest at dawn (ZT0) and dusk (ZT12).
517 ChIP with *N. benthamiana* leaves was performed as described previously (An et al., 2018),
518 with minor changes as below. The samples were cross-linked with 1% (V/V) formaldehyde
519 under a vacuum for 10 min. The cross-linking was quenched by adding glycine to a final
520 concentration of 125 mM and vacuum infiltration for an additional 5 min. The seedlings
521 were rinsed at least three times with cold double distilled water and dried with a paper towel

522 as thoroughly as possible before rapidly freezing the samples in liquid nitrogen. The
523 isolation and sonication of chromatin were performed as described previously (Bowler,
524 2004). GFP-Trap magnetic agarose beads (gtma-20-20rxns, ChromoTek) were used for
525 immunoprecipitation at 4 °C for at least 3 hours. Subsequently, washes with low-salt
526 washing buffer, high salt washing buffer, LiCl washing buffer, and TE buffer were all
527 performed on a magnetic stand. The reverse cross-linking of chromatin was performed by
528 incubating at 65 °C overnight. Both input DNA and ChIPed DNA were purified and analyzed
529 by qPCR. Enrichment of DNA (expressed as % input) was calculated by the following
530 equation: $IP/Input (\%) = 2^{[Ct(Input)-Ct(IP)]} * 100$. All primers used in this assay are listed in
531 Supplemental Table S1.

532 **Immunoblot analysis**

533 For Co-IP assays, *Agrobacteria* harboring *CsVMV:PHYA-HA* and *CsVMV:PHYB-HA*
534 were transiently expressed alone or co-expressed with *35S:GFP-TIC*, *35S: GFP-TIC-NT*, or
535 *35S:GFP-TIC-CT* as noted in the leaves of five-week-old *Nicotiana benthamiana* plants. For
536 Co-IP assay of GFP-TIC with TPL-FLAG, the infiltrated leaves were cross-linked with 1%
537 formaldehyde as previously described (Kim et al., 2011). Total proteins were extracted from
538 the samples with buffer containing 50 mM Tris-HCl, pH 7.5, 150 mM NaCl, 1 mM EDTA,
539 0.1% Nonidet P-40, 1 mM PMSF, 1 mM DTT, and protease inhibitors (5 mg/mL
540 Chymostatin, 5 mg/mL Leupeptin, 5 mg/mL Pepstatin, 5 mg/mL Aprotinin, 50 mM MG132,
541 50 mM MG115, 50 mM ALLN, 2 mM NaF, 2 mM Na₃VO₄). The supernatant was
542 subsequently incubated with GFP-trap beads for 3 h at 4°C. After four washes with protein
543 extraction buffer, the beads were resuspended in 2×SDS-PAGE sample buffer. The samples

544 were heated at 60 °C for 2 min and separated on a SDS-PAGE gel for immunoblot analysis.

545 For protein extraction from Arabidopsis tissues, homozygous *35S:PHYA-YFP* and
546 *35S:PHYA-YFP tic-2* seedlings were grown under constant light or under 12 h light/12 h
547 dark conditions as indicated and harvested over a time course. Total proteins were extracted
548 from the samples in the above buffer. Primary antibodies used in this study include anti-GFP
549 (ab6556, Abcam), anti-HA (11867423001, Roche) anti-FLAG (Abmart), anti-Tubulin
550 (T9026, Sigma) anti-Actin (EASYBIO), anti-phyA and anti-RPN6 (Zhang et al., 2018a), and
551 anti-COP1 (Zhang et al., 2018a).

552 **Yeast Two-Hybrid assay**

553 The LexA-based yeast two-hybrid assay was performed as previously described
554 (Zhang et al., 2018a). Briefly, the *LexA-PHYA-N*, *LexA-PHYA-C1*, *LexA-PHYA-C2* and
555 *AD-TIC*, *AD-TIC-NT*, *AD-TIC-CT* fusion plasmids were co-transformed into yeast strain
556 EGY48, which contains the reporter plasmid *p8op: LacZ* (Clontech). Yeast transformation
557 was performed according to the Yeast Protocols Handbook (Clontech). The co-transformed
558 yeast cells were grown on synthetic dropout (SD) medium without tryptophan and leucine
559 (SD-TL) for 3 days at 30°C. The transformants were then transferred to
560 SD/-Trp/-Leu/-His/-Ade (SDTLHA) medium containing 40 mg/mL X-gal
561 (5-bromo-4-chloro-3-indolyl-b-d-galactopyranoside) for blue color development. The
562 primers used for the yeast two-hybrid assay are listed in Supplemental Table S1.

563 **Bimolecular Fluorescence Complementation assays**

564 For the Bimolecular Fluorescence Complementation (BiFC) assay, the full-length

565 coding sequence of *TIC* was subcloned into *2YC-pBI* and *2YN-pBI*, while the full-length
566 coding sequences of *TPL* and *PHYA* were inserted into *2YN-pBI* and *2YC-pBI*, respectively.
567 All primers used for BiFC are listed in Supplemental Table S1. Agrobacteria containing the
568 above plasmids were transiently expressed in five-week-old *N. benthamiana* leaves as
569 indicated. Agrobacterium containing *H2B-mCherry* was used as a nuclear marker. After
570 incubation for 48-72 h, the signals were examined under a confocal microscope (Olympus
571 FV1000MPE).

572 **Transcriptional Repression Activity Assay in *N. benthamiana***

573 Agrobacteria carrying various fusion expression vectors (Effectors *GFP-TIC*;
574 Reporters *PHYApro:LUC-1300*, *PHYAΔS4pro:LUC-1300*, *PHYAΔS5pro:LUC-1300*,
575 *PHYAΔS6pro:LUC-1300*) were used in the transcriptional repression activity assay. Each
576 reporter vector paired with *GFP-TIC* or *GFP* effectors were co-infiltrated into *N.*
577 *benthamiana* leaves via syringe infiltration as previously described (Li et al., 2019), with
578 *p35S:GUS-HA* as the reference plasmid. The luminescence signals were captured 2 days
579 later using a CCD camera (LN/1300-EB/1, Princeton Instruments). The bioluminescence
580 intensity of the LUC signals was quantified using MetaMorph Microscopy Automation and
581 Image Analysis Software (Molecular Devices), as previously described (Li et al., 2019).

582 **Acquisition of Fluorescent Signals from Nuclear Speckles**

583 To observe the formation of phyA nuclear speckles, *PHYA-YFP* and *PHYA-YAP tic-2*
584 seedlings were grown under constant darkness for 5 days. The samples were kept in the dark,
585 and green light was used when necessary. The nuclear fluorescence intensity of hypocotyls
586 close to the curved hooks was observed. The same magnification and other parameter

587 settings were maintained among different samples. After collecting the fluorescent signals in
588 the dark, the stationary glass slide was exposed to red light or far-red light for the indicated
589 time to acquire the corresponding fluorescent signals. For the same nucleus at different light
590 exposure times, the Intensity Mean Value with the same area was measured using ZEN Blue
591 Lite software. The Intensity Mean Value of each nucleus in the dark was used as a basal
592 control for calculation. The Objective was C-Apochromat 63X/1.2 W Korr UV VIS IR, the
593 laser wavelength was 514 nm and Detector Gain was 790 V, and the fluorescent signals were
594 detected under a Zeiss LSM980 laser-scanning microscope with elyra 7.

595

596 **Nuclear Protein Fractionation**

597 The nuclear protein fractionation experiment was performed as previously described (Wang
598 et al., 2010). Briefly, seedlings grown in continuous darkness at 22 °C on half strength MS
599 with 1% sucrose for 5 days were treated with CHX for 30 min prior to a 15 min light
600 irradiation. 500 mg etiolated seedling tissue was ground into a fine powder in liquid nitrogen
601 and homogenized with 500 µl lysis buffer (20 mM Tris-HCl, pH 7.5, 20 mM KCl, 2 mM
602 EDTA, 2.5 mM MgCl₂, 25% glycerol and 250 mM sucrose, 5 mM DTT, and 1 mM PMSF)
603 supplemented with protease inhibitors (5 mg/mL Chymostatin, 5 mg/mL Leupeptin, 5
604 mg/mL Pepstatin, 5 mg/mL Aprotinin, and 5 mg/mL Antipain). The homogenate was filtered
605 through a double layer of Miracloth. The flow-through was centrifuged at 1500g for 10 min.
606 The precipitates were resuspended in 1 mL of NRBT buffer (20 mM Tris-HCl, pH 7.5, 25%
607 glycerol, 2.5 mM MgCl₂, 0.2% Triton X-100, 1 mM PMSF, and 5 mg/mL protease inhibitors)
608 and were then centrifuged. The above step was repeated twice, and the pellets were

609 resuspended in 500 mL of NRB2 (20 mM Tris-HCl, pH 7.5, 0.25 M sucrose, 10 mM MgCl₂,
610 0.5% Triton X-100, 5 mM β-mercaptoethanol, 1 mM PMSF and 5 mg/mL protease inhibitors)
611 followed by centrifugation; this step was repeated once. The nuclear pellets were finally
612 obtained after centrifuging at 16,000 g for 10 min at 4 °C and resuspended in 90 μl lysis
613 buffer. Histone H3 was used as a nuclear marker for immunoblot analysis.

614 **Bioluminescence Assay and Estimation of the Circadian Period**

615 The *CCAI:LUC* reporter gene was described previously (Wang et al., 2013).
616 Bioluminescence assays were performed as previously described (Wang et al., 2020). To
617 generate *tic-3 CCAI:LUC* lines, *tic-3* was crossed with *CCAI:LUC*, and the homozygous
618 segregants were confirmed in the F2 generation based on bulk F3 genotypes and phenotypes.
619 Screening of homozygous *CCAI:LUC* lines was based 100% kanamycin resistance.
620 Bioluminescence signals were obtained under constant red or blue light conditions as noted.
621 Bioluminescence signals were collected with a CCD camera (LN/1300-EB/1, Princeton
622 Instruments). Raw bioluminescence data were imported into the Biological Rhythms
623 Analysis software system (BRASS version 2.14) (Southern and Millar, 2005) and analyzed
624 with a Fourier transform–nonlinear least-squares suite of programs. Period lengths were
625 estimated as variance-weighted period ± s.e.m. with a time window from 24 to 144 h.

626

627 **Statistical Analysis**

628 The differences between two means were statistically analyzed using a Student's *t*-test.
629 Statistically significant differences were defined as those with $P < 0.05$. Significance levels
630 are indicated as* $P < 0.05$,** $P < 0.01$, and *** $P < 0.001$. To analyze the significance of

631 differences among more than two populations, one-way ANOVA with Tukey's honestly
632 significant difference (HSD) was used. ANOVA was performed using SPSS (Statistical
633 Package for the Social Sciences) software. The symbols above the column represent the
634 number of plants for each sample. The lowercase letters indicate significant differences ($P <$
635 0.05) among the different samples. The methods used for statistical analysis are indicated in
636 the figure legends, and "biological replicates" means that the experiments were performed
637 with different plants. The results of ANOVA and Student's *t*-tests are provided in
638 Supplemental File S1.

639 **Accession Numbers**

640 Sequence data from this article can be found in the Arabidopsis Genome Initiative or
641 GenBank/EMBL databases under the following accession numbers: *TIC* (At3g22380),
642 *PHYA* (At1g09570), *FHY1* (At2g37678), *FHL* (At5g02200), *PAR1* (At2g42870), *PHYB*
643 (At2g18790), *TPL* (At1g15750), *CHR4* (At5g44800), *SSRP1* (At3g28730), *PILI*
644 (At2g46970), *HB2* (At3g10520), *COPI* (At2g32950). The RNA-seq raw data have been
645 deposited in the NCBI SRA database under accession number GSE156016.

646 **Supplemental Data**

647 **Supplemental Figure S1.** Hypocotyl growth of *tic-2* under photoperiodic and continuous
648 dark conditions.

649 **Supplemental Figure S2.** Flowering time and circadian phenotypes of *tic-3*.

650 **Supplemental Figure S3.** Hypocotyl phenotypes and fluence response curves of *tic-3* for
651 FRc, Rc, and Bc

652 **Supplemental Figure S4.** Hypocotyl growth of *tic-3* under photoperiodic and continuous
653 dark conditions.

654 **Supplemental Figure S5.** *TICpro:GFP-TIC* genetically rescues the hypocotyl defects of
655 *tic-2*.

656 **Supplemental Figure S6.** RNA-Sequencing analysis of the *tic-2* mutant.

657 **Supplemental Figure S7.** Gene Ontology analysis of DEGs in the *tic-2* mutant.

658 **Supplemental Figure S8.** Overlapping DEGs at pre-dawn vs. post-dusk in the *tic-2* mutant.

659 **Supplemental Figure S9.** Venn diagrams showing the overlapping genes between phyA
660 direct targets and upregulated or downregulated DEGs in *tic-2* at post-dusk.

661 **Supplemental Figure S10.** Validating the transcript levels of the genes that are oppositely
662 regulated by TIC and phyA in *tic-2* and *phyA-211*, as determined by time-course RT-qPCR.

663 **Supplemental Figure S11.** Validating the transcript levels of FR signaling components in
664 *tic-3*.

665 **Supplemental Figure S12.** Transcript level of *PHYA* in *tic-2* under constant light conditions.

666 **Supplemental Figure S13.** Additional biological repeat of the ChIP-qPCR assay with
667 *TICpro:GFP-TIC* seedlings.

668 **Supplemental Figure S14.** TOC1 does not associate with the *PHYA* promoter.

669 **Supplemental Figure S15.** Additional biological repeat of RT-qPCR to measure *PHYA*
670 transcript levels in *tic-2* vs. Col-0 in constant darkness and after transfer to red light.

671 **Supplemental Figure S16.** Transient repression assay of TIC on the *PHYA* promoter lacking
672 the S4, S5, or S6 region.

673 **Supplemental Figure S17.** The putative EAR domain of TIC is required for TIC to interact
674 with TPL.

675 **Supplemental Figure S18.** ChIP-qPCR assay of TPL on the *PHYA* promoter.

676 **Supplemental Figure S19.** TPL marginally facilitates the repression of *PHYA* transcription
677 by TIC.

678 **Supplemental Figure S20.** PHYA protein stability in *tic-2* in the absence of sucrose.

679 **Supplemental Figure S21.** Nuclear speckle formation of PHYA-YFP increases in *tic-2* upon
680 FR or R light irradiation.

681 **Supplemental Figure S22.** Total and nuclear PHYA-YFP protein abundance in *PHYA-YFP*
682 and *PHYA-YFP tic-2*.

683 **Supplemental Figure S23.** Photoperiodic hypocotyl growth phenotype of *tic-2 phyA-211*.

684 **Supplemental Figure S24.** Protein abundance of COP1 and PHYA in Col-0 and *tic-2* grown
685 in continuous FR or R light.

686 **Supplemental Table S1.** The primers used in this study.

687 **Supplemental Data Set S1.** DEGs identified in *tic-2* at pre-dawn and post-dusk

688 **Supplemental Data Set S2.** Interactors of TIC identified by IP-MS

689 **Supplemental File S1.** Summary of statistical analyses

690 **ACKNOWLEDGMENTS**

691 We thank Dr. Zhuang Lu and Ms. Jingquan Li from the Plant Science Facility of the
692 Institute of Botany, Chinese Academy of Sciences for their excellent technical assistance on
693 mass spectrometry and confocal microscopy, respectively. We thank Dr. Lin Li (Fudan

694 University) for sharing *35S:PHYA-YFP* transgenic seeds.

695 This work was supported by the Strategic Priority Research Program of the Chinese
696 Academy of Sciences (Grant No. XDB27030206), the National Natural Science Foundation
697 of China (31770287) and (to L.W.), and a BBSRC grant (BB/V006665/1) to S. J.D.

698 **Author contributions**

699 Y.W., C.S., Y.J.Y., Y.Q.H., H.W., N.L., H.L., J.D., and B.L. performed the research. J.G.L.,
700 S.J.D., and L.W. designed the experiments and analyzed the data. Y.W., S.J.D., and L.W.
701 wrote the paper.

702 **Conflict of Interest**

703 The authors declare no competing interests.

704 **References**

- 705 **Abe, H., Yamamoto, K.T., Nagatani, A., and Furuya, M.** (1985). Characterization Of Green Tissue-Specific
706 Phytochrome Isolated Immunochemically From Pea-Seedlings. *Plant And Cell Physiology* **26**,
707 1387-1399.
- 708 **An, J.P., Wang, X.F., Li, Y.Y., Song, L.Q., Zhao, L.L., You, C.X., and Hao, Y.J.** (2018). EIN3-LIKE1, MYB1, and
709 ETHYLENE RESPONSE FACTOR3 Act in a Regulatory Loop That Synergistically Modulates Ethylene
710 Biosynthesis and Anthocyanin Accumulation. *Plant Physiol* **178**, 808-823.
- 711 **Casal, J.J., Candia, A.N., and Sellaro, R.** (2014). Light perception and signalling by phytochrome A. *J Exp Bot*
712 **65**, 2835-2845.
- 713 **Chen, F., Li, B.S., Li, G., Charron, J.B., Dai, M.Q., Shi, X.R., and Deng, X.W.** (2014). Arabidopsis Phytochrome A
714 Directly Targets Numerous Promoters for Individualized Modulation of Genes in a Wide Range of
715 Pathways. *Plant Cell* **26**, 1949-1966.
- 716 **Clough, S.J., and Bent, A.F.** (1998). Floral dip: a simplified method for Agrobacterium-mediated
717 transformation of *Arabidopsis thaliana*. *The Plant journal : for cell and molecular biology* **16**, 735-743.
- 718 **Debrieux, D., Trevisan, M., and Fankhauser, C.** (2013). Conditional involvement of constitutive
719 photomorphogenic1 in the degradation of phytochrome A. *Plant Physiol* **161**, 2136-2145.
- 720 **Ding, Z., Millar, A.J., Davis, A.M., and Davis, S.J.** (2007). TIME FOR COFFEE encodes a nuclear regulator in the
721 *Arabidopsis thaliana* circadian clock. *Plant Cell* **19**, 1522-1536.
- 722 **Fankhauser, C.** (2001). The phytochromes, a family of Red/Far-red absorbing photoreceptors. *Journal Of*
723 *Biological Chemistry* **276**, 11453-11456.

724 **Hall, A., Bastow, R.M., Davis, S.J., Hanano, S., McWatters, H.G., Hibberd, V., Doyle, M.R., Sung, S., Halliday,**
725 **K.J., Amasino, R.M., and Millar, A.J.** (2003). The TIME FOR COFFEE gene maintains the amplitude and
726 timing of Arabidopsis circadian clocks. *Plant Cell* **15**, 2719-2729.

727 **Hong, L.W., Yan, D.W., Liu, W.C., Chen, H.G., and Lu, Y.T.** (2014). TIME FOR COFFEE controls root meristem
728 size by changes in auxin accumulation in Arabidopsis. *J Exp Bot* **65**, 275-286.

729 **Ito, J., Fukaki, H., Onoda, M., Li, L., Li, C., Tasaka, M., and Furutani, M.** (2016). Auxin-dependent
730 compositional change in Mediator in ARF7- and ARF19-mediated transcription. *P Natl Acad Sci USA*
731 **113**, 6562-6567.

732 **Kim, T.S., Kim, W.Y., Fujiwara, S., Kim, J., Cha, J.Y., Park, J.H., Lee, S.Y., and Somers, D.E.** (2011). HSP90
733 functions in the circadian clock through stabilization of the client F-box protein ZEITLUPE.
734 *Proceedings Of the National Academy Of Sciences Of the United States Of America* **108**,
735 16843-16848.

736 **Kircher, S., Kozma-Bognar, L., Kim, L., Adam, E., Harter, K., Schafer, E., and Nagy, F.** (1999). Light
737 quality-dependent nuclear import of the plant photoreceptors phytochrome A and B. *Plant Cell* **11**,
738 1445-1456.

739 **Kircher, S., Gil, P., Kozma-Bognar, L., Fejes, E., Speth, V., Husselstein-Muller, T., Bauer, D., Adam, E., Schafer,**
740 **E., and Nagy, F.** (2002). Nucleocytoplasmic partitioning of the plant photoreceptors phytochrome A,
741 B, C, D, and E is regulated differentially by light and exhibits a diurnal rhythm. *Plant Cell* **14**,
742 1541-1555.

743 **Kolmos, E., Herrero, E., Bujdoso, N., Millar, A.J., Toth, R., Gyula, P., Nagy, F., and Davis, S.J.** (2011). A
744 reduced-function allele reveals that EARLY FLOWERING3 repressive action on the circadian clock is
745 modulated by phytochrome signals in Arabidopsis. *Plant Cell* **23**, 3230-3246.

746 **Li, B., Wang, Y., Zhang, Y., Tian, W., Chong, K., Jang, J.C., and Wang, L.** (2019). PRR5, 7 and 9 positively
747 modulate TOR signaling-mediated root cell proliferation by repressing TANDEM ZINC FINGER 1 in
748 Arabidopsis. *Nucleic Acids Res* **47**, 5001-5015.

749 **Li, N., Zhang, Y., He, Y., Wang, Y., and Wang, L.** (2020). Pseudo Response Regulators regulate photoperiodic
750 hypocotyl growth by repressing PIF4/5 transcription. *Plant Physiol* **183**, 686-699.

751 **Liu, H., Yu, X., Li, K., Klejnot, J., Yang, H., Lisiero, D., and Lin, C.** (2008). Photoexcited CRY2 interacts with CIB1
752 to regulate transcription and floral initiation in Arabidopsis. *Science* **322**, 1535-1539.

753 **Long, J.A., Ohno, C., Smith, Z.R., and Meyerowitz, E.M.** (2006). TOPLESS regulates apical embryonic fate in
754 Arabidopsis. *Science* **312**, 1520-1523.

755 **Ma, X.L., Zhang, Q.Y., Zhu, Q.L., Liu, W., Chen, Y., Qiu, R., Wang, B., Yang, Z.F., Li, H.Y., Lin, Y.R., Xie, Y.Y.,**
756 **Shen, R.X., Chen, S.F., Wang, Z., Chen, Y.L., Guo, J.X., Chen, L.T., Zhao, X.C., Dong, Z.C., and Liu, Y.G.**
757 (2015). A Robust CRISPR/Cas9 System for Convenient, High-Efficiency Multiplex Genome Editing in
758 Monocot and Dicot Plants. *Molecular Plant* **8**, 1274-1284.

759 **Martin-Arevalillo, R., Nanao, M.H., Larrieu, A., Vinos-Poyo, T., Mast, D., Galvan-Ampudia, C., Brunoud, G.,**
760 **Vernoux, T., Dumas, R., and Parcy, F.** (2017). Structure of the Arabidopsis TOPLESS corepressor
761 provides insight into the evolution of transcriptional repression. *P Natl Acad Sci USA* **114**, 8107-8112.

762 **McClung, C.R.** (2019). The Plant Circadian Oscillator. *Biology (Basel)* **8**, 14.

763 **Nagatani, A.** (2004). Light-regulated nuclear localization of phytochromes. *Curr Opin Plant Biol* **7**, 708-711.

764 **Nohales, M.A., and Kay, S.A.** (2016). Molecular mechanisms at the core of the plant circadian oscillator. *Nat*
765 *Struct Mol Biol* **23**, 1061-1069.

766 **Pauwels, L., Barbero, G.F., Geerinck, J., Tilleman, S., Grunewald, W., Perez, A.C., Chico, J.M., Bossche, R.V.,**
767 **Sewell, J., Gil, E., Garcia-Casado, G., Witters, E., Inze, D., Long, J.A., De Jaeger, G., Solano, R., and**

768 **Goossens, A.** (2010). NINJA connects the co-repressor TOPLESS to jasmonate signalling. *Nature* **464**,
769 788-791.

770 **Robinson, J.T., Thorvaldsdottir, H., Winckler, W., Guttman, M., Lander, E.S., Getz, G., and Mesirov, J.P.**
771 (2011). Integrative genomics viewer. *Nature biotechnology* **29**, 24-26.

772 **Sanchez-Villarreal, A., Davis, A.M., and Davis, S.J.** (2018). AKIN10 activity as a cellular link between
773 metabolism and circadian-clock entrainment in *Arabidopsis thaliana*. *Plant Signal Behav* **13**,
774 e1411448.

775 **Sanchez-Villarreal, A., Shin, J., Bujdoso, N., Obata, T., Neumann, U., Du, S.X., Ding, Z., Davis, A.M., Shindo,**
776 **T., Schmelzer, E., Sulpice, R., Nunes-Nesi, A., Stitt, M., Fernie, A.R., and Davis, S.J.** (2013). TIME FOR
777 COFFEE is an essential component in the maintenance of metabolic homeostasis in *Arabidopsis*
778 *thaliana*. *Plant J* **76**, 188-200.

779 **Sanchez, S.E., Rugnone, M.L., and Kay, S.A.** (2020). Light Perception: A Matter of Time. *Mol Plant* **13**,
780 363-385.

781 **Seaton, D.D., Toledo-Ortiz, G., Ganpudi, A., Kubota, A., Imaizumi, T., and Halliday, K.J.** (2018). Dawn and
782 photoperiod sensing by phytochrome A. *Proc Natl Acad Sci U S A* **115**, 10523-10528.

783 **Seo, H.S., Watanabe, E., Tokutomi, S., Nagatani, A., and Chua, N.H.** (2004). Photoreceptor ubiquitination by
784 COP1 E3 ligase desensitizes phytochrome A signaling. *Genes & Development* **18**, 617-622.

785 **Shalit-Kaneh, A., Kumimoto, R.W., Filkov, V., and Harmer, S.L.** (2018). Multiple feedback loops of the
786 *Arabidopsis* circadian clock provide rhythmic robustness across environmental conditions. *P Natl*
787 *Acad Sci USA* **115**, 7147-7152.

788 **Shanklin, J., Jabben, M., and Vierstra, R.D.** (1987). Red Light-Induced Formation Of Ubiquitin-Phytochrome
789 Conjugates - Identification Of Possible Intermediates Of Phytochrome Degradation. *Proc Natl Acad*
790 *Sci U S A* **84**, 359-363.

791 **Sharrock, R.A., and Clack, T.** (2002). Patterns of expression and normalized levels of the five *Arabidopsis*
792 phytochromes. *Plant Physiol* **130**, 442-456.

793 **Shin, J., Heidrich, K., Sanchez-Villarreal, A., Parker, J.E., and Davis, S.J.** (2012). TIME FOR COFFEE represses
794 accumulation of the MYC2 transcription factor to provide time-of-day regulation of jasmonate
795 signaling in *Arabidopsis*. *Plant Cell* **24**, 2470-2482.

796 **Shin, J., Sanchez-Villarreal, A., Davis, A.M., Du, S.X., Berendzen, K.W., Koncz, C., Ding, Z., Li, C., and Davis,**
797 **S.J.** (2017). The metabolic sensor AKIN10 modulates the *Arabidopsis* circadian clock in a
798 light-dependent manner. *Plant Cell Environ* **40**, 997-1008.

799 **Somers, D.E., Devlin, P.F., and Kay, S.A.** (1998). Phytochromes and cryptochromes in the entrainment of the
800 *Arabidopsis* circadian clock. *Science* **282**, 1488-1490.

801 **Southern, M.M., and Millar, A.J.** (2005). Circadian genetics in the model higher plant, *Arabidopsis thaliana*.
802 *Methods Enzymol* **393**, 23-35.

803 **Thorvaldsdottir, H., Robinson, J.T., and Mesirov, J.P.** (2013). Integrative Genomics Viewer (IGV):
804 high-performance genomics data visualization and exploration. *Briefings in bioinformatics* **14**,
805 178-192.

806 **Toth, R., Kevei, E., Hall, A., Millar, A.J., Nagy, F., and Kozma-Bognar, L.** (2001). Circadian clock-regulated
807 expression of phytochrome and cryptochrome genes in *Arabidopsis*. *Plant Physiol* **127**, 1607-1616.

808 **Trapnell, C., Williams, B.A., Pertea, G., Mortazavi, A., Kwan, G., van Baren, M.J., Salzberg, S.L., Wold, B.J.,**
809 **and Pachter, L.** (2010). Transcript assembly and quantification by RNA-Seq reveals unannotated
810 transcripts and isoform switching during cell differentiation. *Nature biotechnology* **28**, 511-515.

811 **von Arnim, A.G., and Deng, X.W.** (1994). Light inactivation of *Arabidopsis* photomorphogenic repressor COP1

812 involves a cell-specific regulation of its nucleocytoplasmic partitioning. *Cell* **79**, 1035-1045.

813 **von Arnim, A.G., Osterlund, M.T., Kwok, S.F., and Deng, X.W.** (1997). Genetic and developmental control of
814 nuclear accumulation of COP1, a repressor of photomorphogenesis in Arabidopsis. *Plant Physiol* **114**,
815 779-788.

816 **Wang, L., Fujiwara, S., and Somers, D.E.** (2010). PRR5 regulates phosphorylation, nuclear import and
817 subnuclear localization of TOC1 in the Arabidopsis circadian clock. *EMBO J* **29**, 1903-1915.

818 **Wang, L., Kim, J., and Somers, D.E.** (2013). Transcriptional corepressor TOPLESS complexes with
819 pseudoresponse regulator proteins and histone deacetylases to regulate circadian transcription. *P*
820 *Natl Acad Sci USA* **110**, 761-766.

821 **Wang, Y., He, Y., Su, C., Zentella, R., Sun, T.P., and Wang, L.** (2020). Nuclear Localized O-Fucosyltransferase
822 SPY Facilitates PRR5 Proteolysis to Fine-Tune the Pace of Arabidopsis Circadian Clock. *Mol Plant* **13**,
823 446-458.

824 **Wenden, B., Kozma-Bognar, L., Edwards, K.D., Hall, A.J., Locke, J.C., and Millar, A.J.** (2011). Light inputs
825 shape the Arabidopsis circadian system. *Plant J* **66**, 480-491.

826 **Yang, C., Xie, F., Jiang, Y., Li, Z., Huang, X., and Li, L.** (2018). Phytochrome A Negatively Regulates the Shade
827 Avoidance Response by Increasing Auxin/Indole Acetic Acid Protein Stability. *Dev Cell* **44**, 29-41 e24.

828 **Zhang, S., Li, C., Zhou, Y., Wang, X., Li, H., Feng, Z., Chen, H., Qin, G., Jin, D., Terzaghi, W., Gu, H., Qu, L.J.,
829 Kang, D., Deng, X.W., and Li, J.** (2018a). TANDEM ZINC-FINGER/PLUS3 Is a Key Component of
830 Phytochrome A Signaling. *Plant Cell* **30**, 835-852.

831 **Zhang, Y., Wang, Y., Wei, H., Li, N., Tian, W., Chong, K., and Wang, L.** (2018b). Circadian Evening Complex
832 Represses Jasmonate-Induced Leaf Senescence in Arabidopsis. *Mol Plant* **11**, 326-337.

833 **Zhu, J.Y., Oh, E., Wang, T., and Wang, Z.Y.** (2016). TOC1-PIF4 interaction mediates the circadian gating of
834 thermoresponsive growth in Arabidopsis. *Nat Commun* **7**, 13692.

835

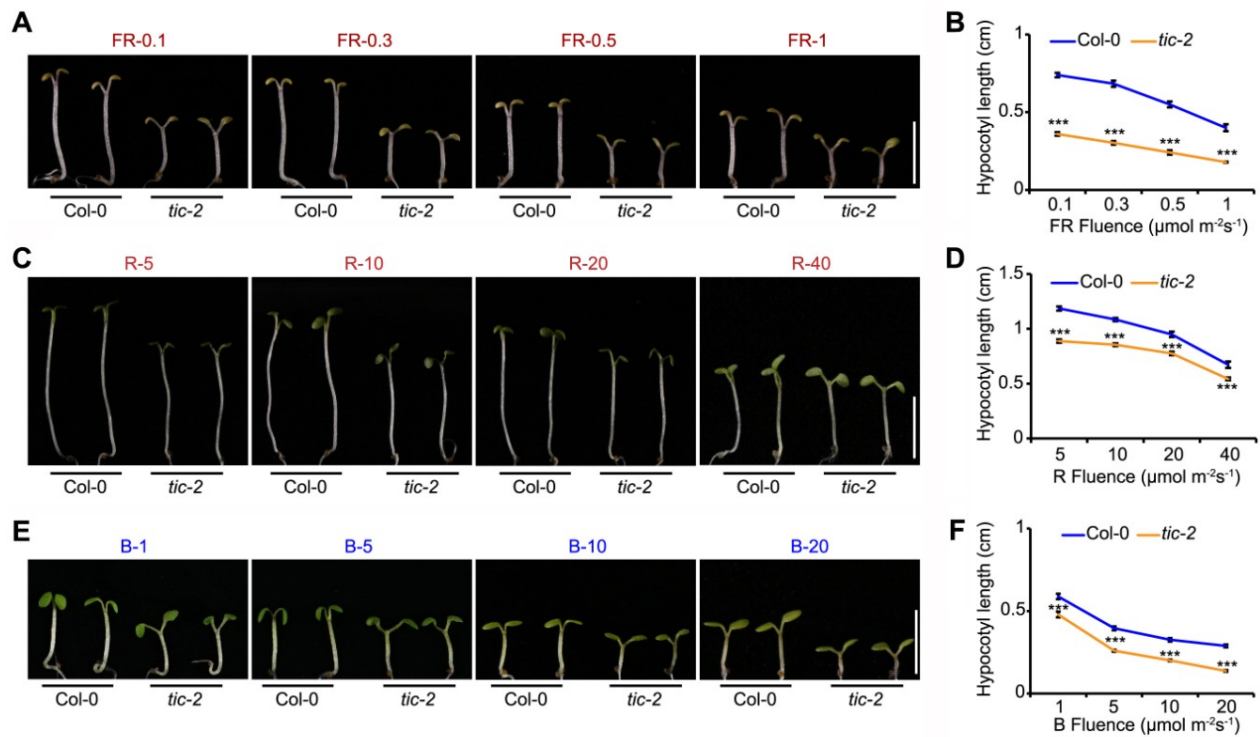


Figure 1. Hypocotyl phenotypes and fluence response curves of *tic-2* under constant far red, red, and blue light.

(A), (C) and (E) Hypocotyl phenotypes of Col-0 and *tic-2*. Seedlings were grown under far red light (FR ~0.1, 0.3, 0.5, and 1 $\mu\text{mol m}^{-2}\text{s}^{-1}$), red light (R ~5, 10, 20, and 40 $\mu\text{mol m}^{-2}\text{s}^{-1}$) or blue light (B ~1, 5, 10, and 20 $\mu\text{mol m}^{-2}\text{s}^{-1}$) for 5 days. Representative seedlings are shown. Bars = 5 mm.

(B), (D) and (F) Fluence response curves of *tic-2* under constant FR, R, and B blue light for the seedlings shown in (A), (C) and (E), respectively; data represent mean \pm s.e.m. ($n \geq 15$), and the asterisks indicate significant difference, according to Student's *t*-test (***) $p < 0.001$.

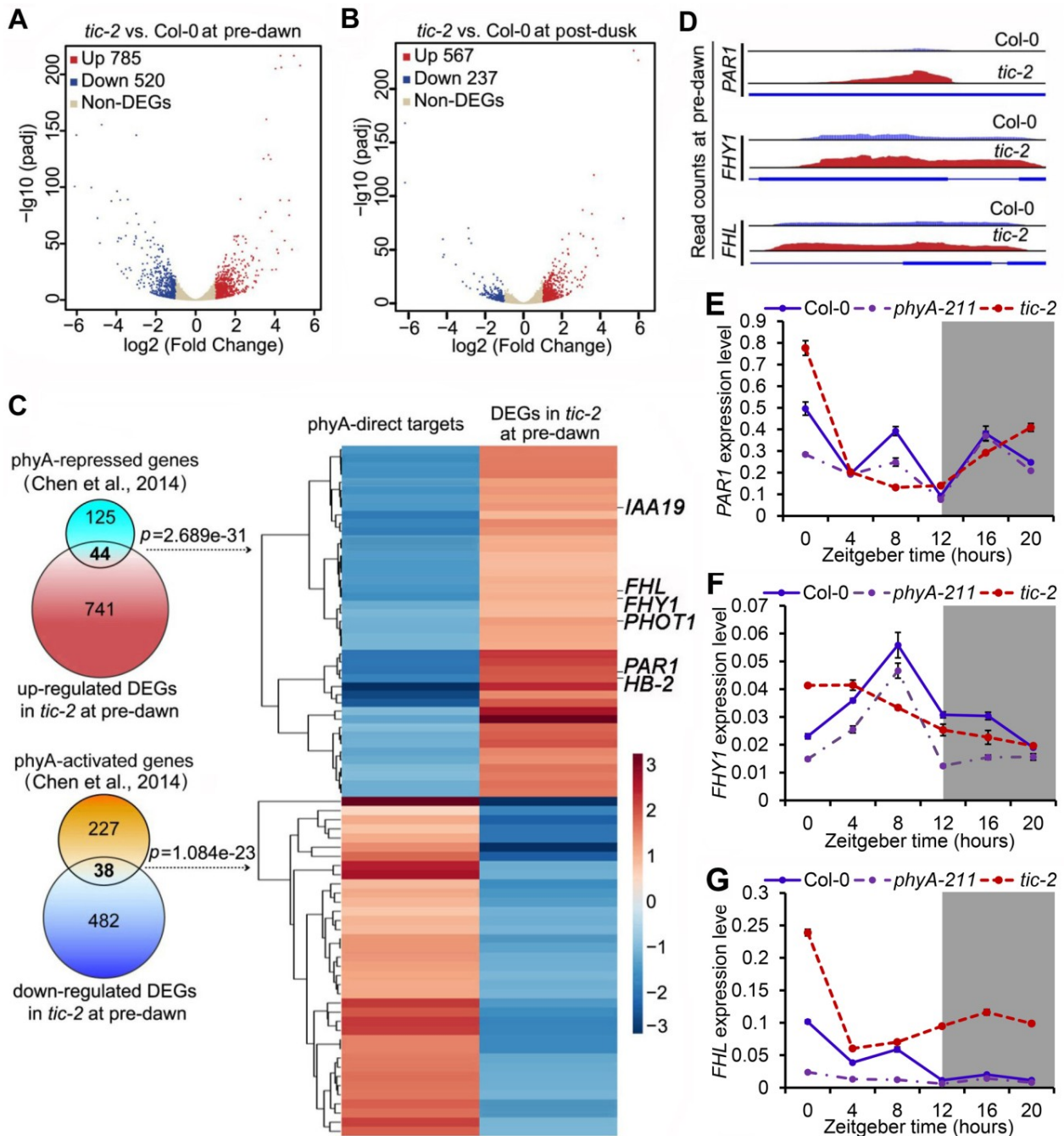


Figure 2. TIC and phyA regulate the transcription of a subset of genes in an opposite manner.

(A) and (B) Volcano plots showing significantly up-regulated (red dots, $p < 0.05$) or down-regulated (blue dots, $p < 0.05$) differentially expressed genes (DEGs) in *tic-2* at pre-dawn (10 min before lights on) (A) or post-dusk (10 min after lights off) (B). The x axis represents the value of \log_2 fold change of *tic-2* against Col-0, and the y axis shows the adjusted $-\log_{10}$ of the p value for the DEGs.

(C) Venn diagram showing the number of overlapping genes between phyA direct targets (Chen, et al., 2014) and DEGs in *tic-2* at pre-dawn. The p values were calculated according to hypergeometric test. The heatmap in the right panel shows the hierarchical clustering of the target genes that were co-regulated by phyA and TIC. Scale represents fold change.

(D) Visualization of RNA-seq raw read counts for *PAR1*, *FHY1* and *FHL* using Integrative Genomics Viewer browser.

(E-G) Transcript levels of *PAR1* (E), *FHY1* (F) and *FHL* (G) in *phyA-211* and *tic-2* under LD conditions. Gene expression levels were normalized by the geometric mean of *ACT2* and *PP2A*. Data represent mean \pm s.e.m (n = 3, biological replicates).

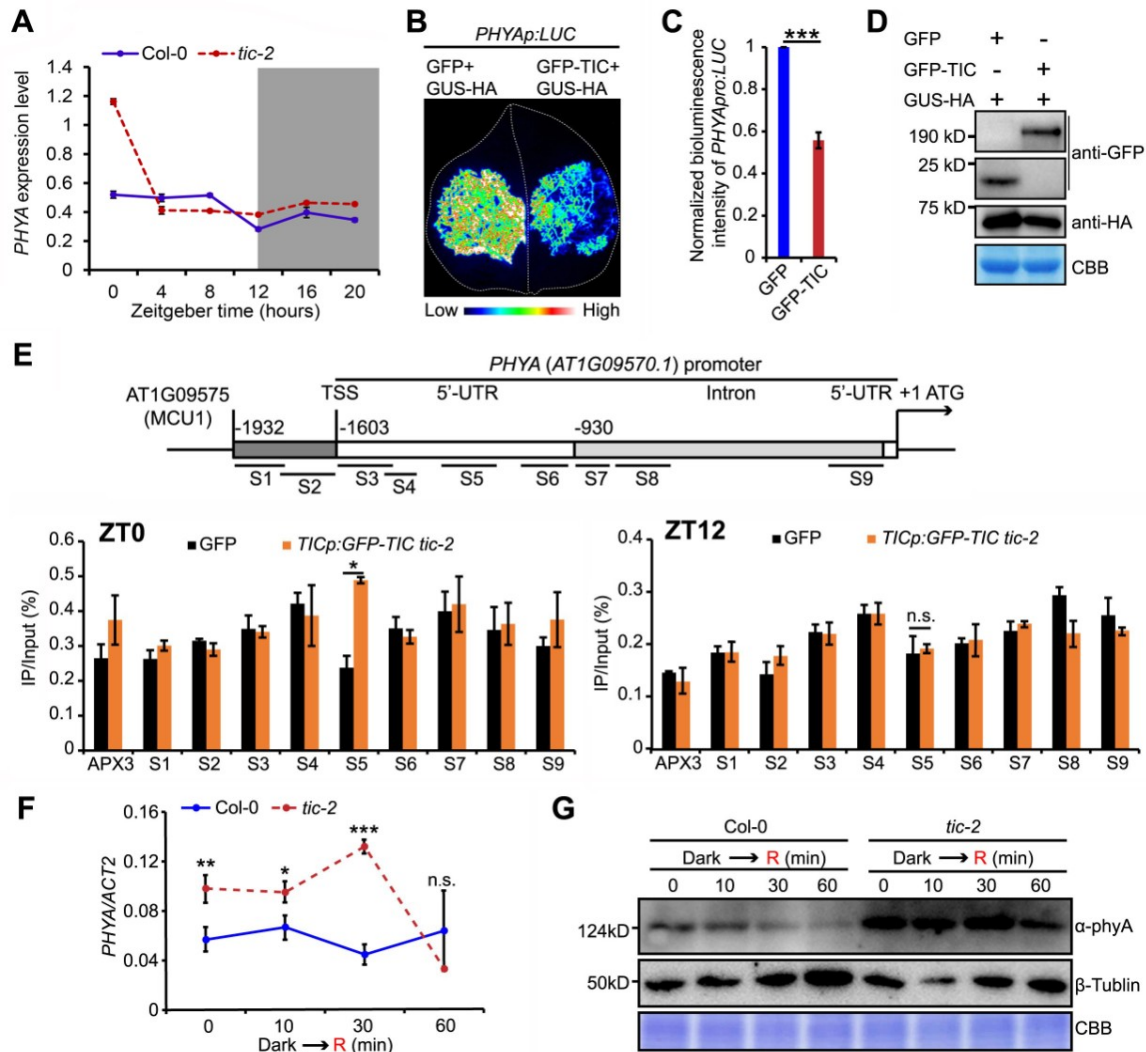


Figure 3. TIC represses *PHYA* transcription mainly at dawn.

- 30 (A) Time course RT-qPCR showing that *PHYA* transcript levels increase in *tic-2* predominantly at pre-dawn. Gene expression levels were normalized by the geometric mean of *ACT2* and *PP2A*. Data represent mean \pm s.e.m. ($n = 3$, biological replicates).
- (B) Representative image of *PHYA*_{pro}:*LUC* co-infiltrated with 35S:*GFP* or 35S:*GFP-TIC* in *N. benthamiana*, with *pGUS-HA* as a reference plasmid.
- 35 (C) Quantification of bioluminescence signals of *PHYA*_{pro}:*LUC* co-infiltrated with 35S:*GFP* or 35S:*GFP-TIC* in *N. benthamiana*. Data represent mean \pm s.e.m. ($n = 9$), and the asterisks indicate significant difference, according to Student's *t*-test ($***p < 0.001$).
- (D) Immunoblot detecting the respective protein levels in (B).
- (E) ChIP assays of 35S:*GFP* and *TIC*_{pro}:*GFP-TIC tic-2* using tissues harvested at dawn (ZT0) and dusk (ZT12). The locations of the amplicons used in the ChIP assay are shown in the upper diagram. Data represent mean \pm s.e.m. ($*p < 0.05$ and n.s. indicates no significant difference ($p > 0.05$), according to Student's *t*-test). The experiments were performed at least twice with similar results.
- 40 (F) RT-qPCR showing that *PHYA* transcript levels were higher in *tic-2* vs. Col-0 in constant darkness and decreased after transfer to an acute pulse of R for 60 min. Data represent mean \pm s.e.m. ($n = 3$, technical replicates). Asterisks indicate significant difference ($*p < 0.05$, $**p < 0.01$ and $***p < 0.001$) and n.s. indicates no significant difference ($p > 0.05$), as determined by Student's *t*-test. The experiments were conducted twice with similar results.
- 45 (G) Immunoblot with *PHYA* antibody in *tic-2* and Col-0 under the indicated light conditions (CBB: Coomassie Brilliant Blue).

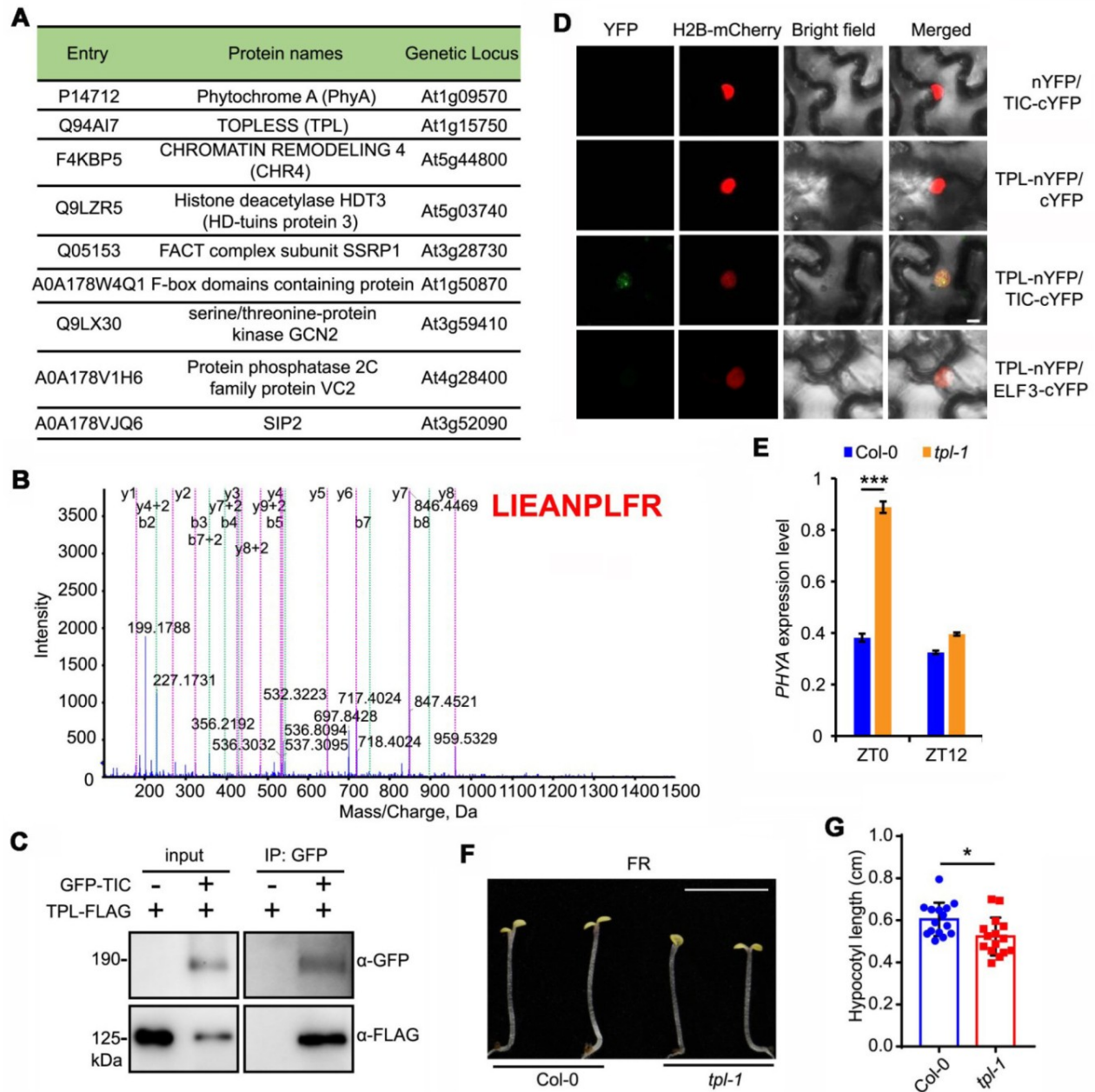


Figure 4. TPL interacts with TIC to repress *PHYA* transcription.

(A) List of the nuclear proteins identified by affinity-purification followed by mass spectrometry (AP-MS) with GFP-TIC. Samples were collected at pre-dawn.

(B) Spectrum of a representative peptide of TPL protein identified by AP-MS.

(C) Co-immunoprecipitation analysis showing that GFP-TIC interacts with TPL-FLAG. Total proteins were extracted from transiently co-infiltrated *N. benthamiana* leaves as indicated. The immunoprecipitation was performed with GFP-Trap beads.

(D) Physical interaction between TIC-cYFP and TPL-nYFP detected in the nucleus in a BiFC assay. H2B-mCherry is a nuclear marker. Scale bar = 5 μ m.

(E) RT-qPCR assay showing the transcript level of *PHYA* is higher in *tpl-1* at ZT0 but not ZT12. Gene expression levels were normalized by the geometric mean of *ACT2* and *PP2A*. Data represent mean \pm s.e.m. ($n = 3$, biological replicates). Asterisks indicate significant difference, according to Student's *t*-test (*** $p < 0.001$).

(F-G) Hypocotyl phenotypes of Col-0 and *tpl-1* grown in continuous FR light (FR $\sim 1 \mu\text{mol m}^{-2} \text{s}^{-1}$). Data represent mean \pm s.e.m. ($n \geq 15$, * $p < 0.05$ according to Student's *t*-test). Scale bar = 5 mm.

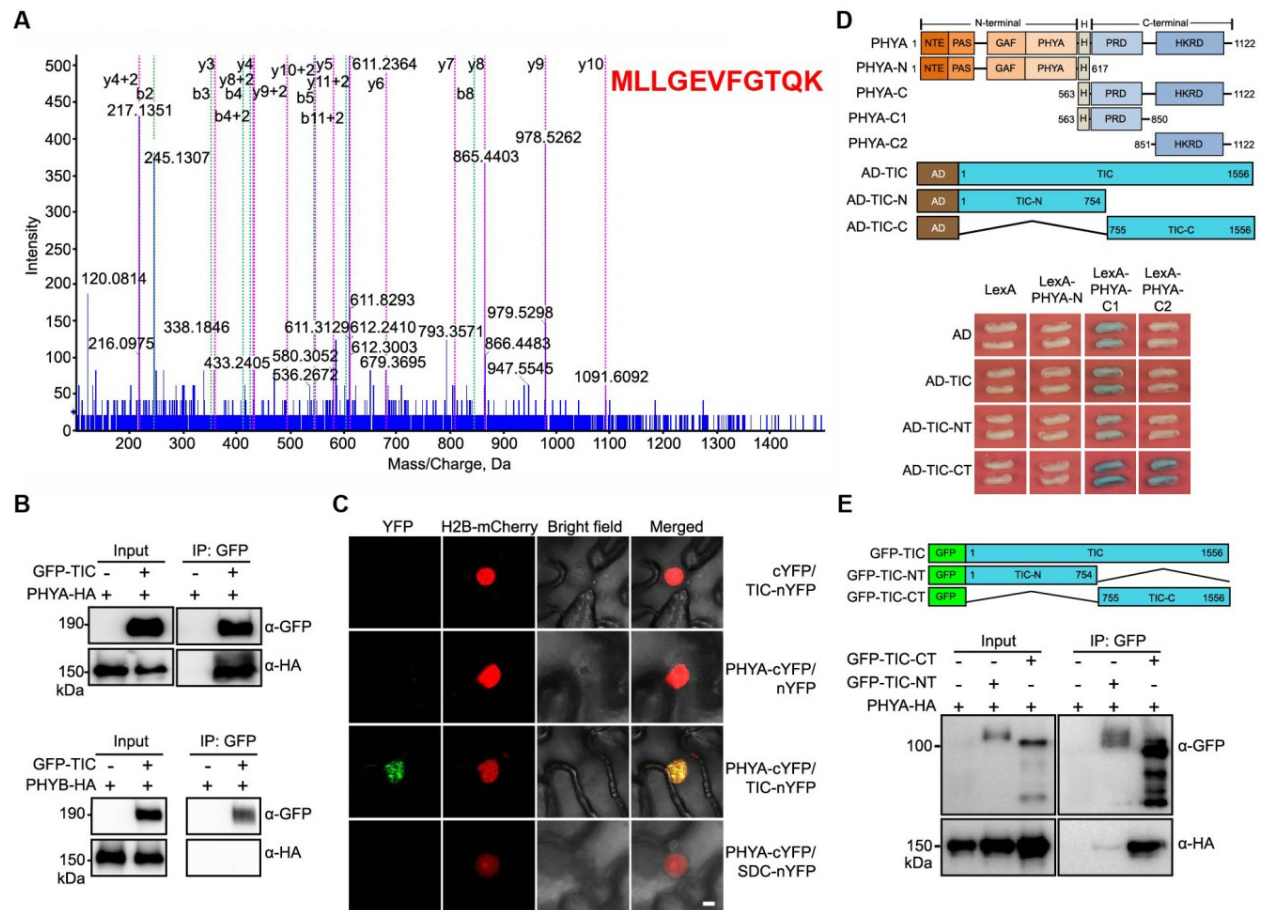


Figure 5. TIC physically interacts with phyA in the nucleus.

- (A) Spectrum of a representative peptide of phyA protein identified by AP-MS with GFP-TIC.
- 70 (B) Co-immunoprecipitation analysis showing that GFP-TIC interacts with PHYA-HA but not PHYB-HA. GFP-Trap beads were used to precipitate protein complexes that were extracted from co-infiltrated *N. benthamiana* leaves as indicated.
- (C) BiFC assay showing that TIC physically interacts with phyA in the nucleus. H2B-mCherry was used as a nuclear marker. Scale bar = 10 μ m.
- 75 (D) Yeast two-hybrid assays showing that the TIC C terminus mediates the interaction with phyA. The constructs used in the yeast two-hybrid assays are shown in the upper diagram.
- (E) Co-immunoprecipitation assay showing a stronger interaction between TIC C terminus and phyA. The constructs of TIC used in the Co-IP assays are shown in the upper diagram.

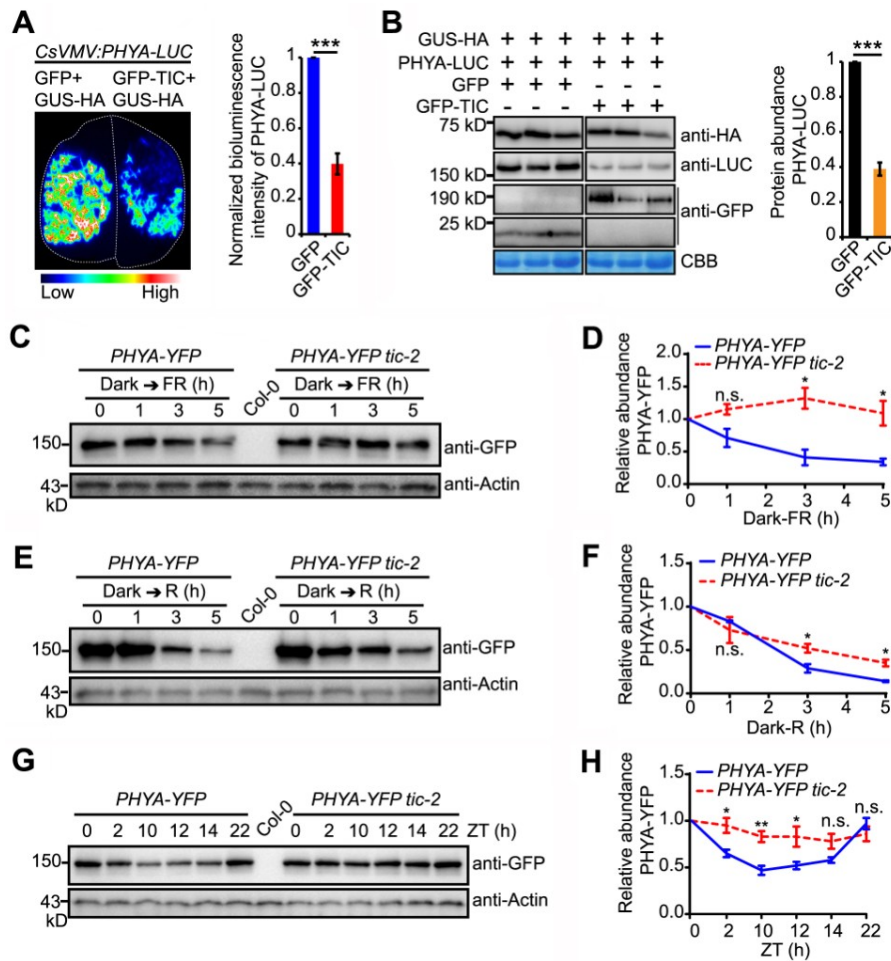


Figure 6. TIC facilitates the light-promoted proteolysis of phyA.

(A) Bioluminescence imaging and intensity quantification of *CsVMV:PHYA-LUC* transiently co-infiltrated with *GFP* or *GFP-TIC* in *N. benthamiana* leaves, with *pGUS-HA* as a reference plasmid. Data represent mean \pm s.e.m. ($n = 13$), and the asterisks indicate significant difference, according to Student's *t*-test ($***p < 0.001$).

(B) Immunoblot detecting the respective protein levels in (A). Data represent mean \pm s.e.m. ($n = 3$), $***p < 0.001$, as determined by Student *t*-test. CBB, Coomassie Brilliant Blue-stained gel.

(C) and (E) Immunoblots showing PHYA-YFP protein in 7-day-old etiolated seedlings of *PHYA-YFP* and *PHYA-YFP tic-2* after transferring to FR or R for the indicated time points.

(D) and (F) Quantitative analysis of PHYA-YFP protein levels as shown in (C) and (E), respectively. Data represent means \pm s.e.m from three biological replicates, asterisks indicate significant difference ($*p < 0.05$) and n.s. indicates no significant difference ($p > 0.05$), according to Student's *t*-test.

PHYA-YFP protein abundance was detected with GFP antibody, Col-0 served as a negative control. Actin antibody was used as a loading control.

(G) Immunoblot of PHYA-YFP protein in seedlings grown under LD conditions.

(H) Quantitative analysis the protein abundance of PHYA-YFP relative to Actin. Data represent means \pm s.e.m from three biological replicates, asterisk indicates significant difference ($*p < 0.05$, $**p < 0.01$) and n.s.

indicates no significant difference ($p > 0.05$), as determined by Student's *t*-test. PHYA-YFP protein abundance was detected with GFP antibody, Col-0 served as a negative control. Actin antibody was used as a loading control.

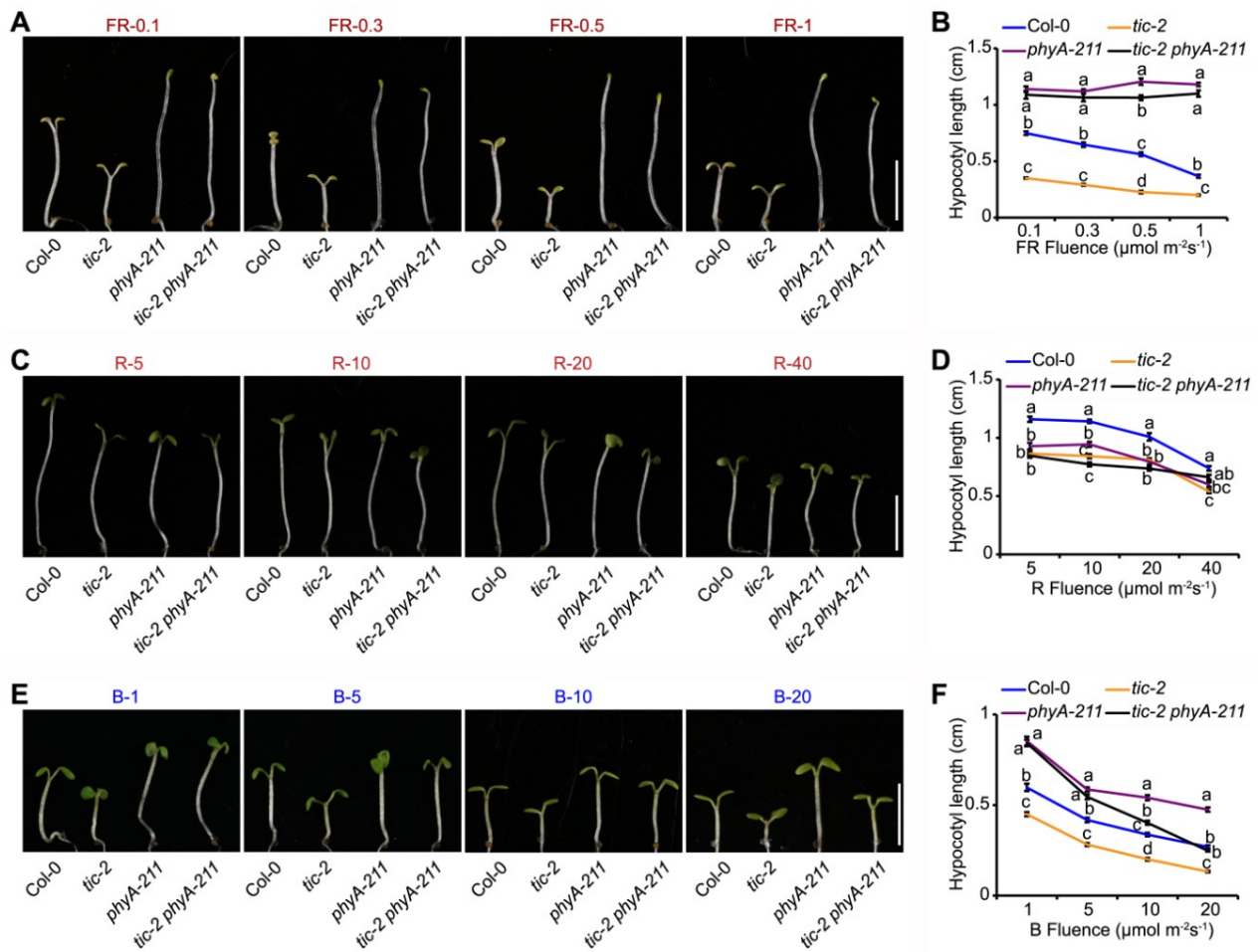
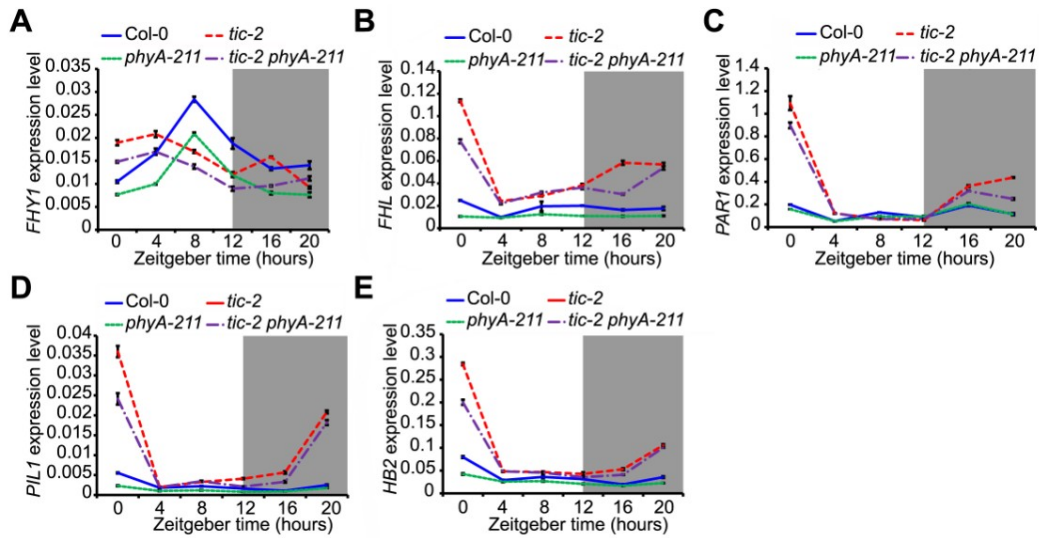


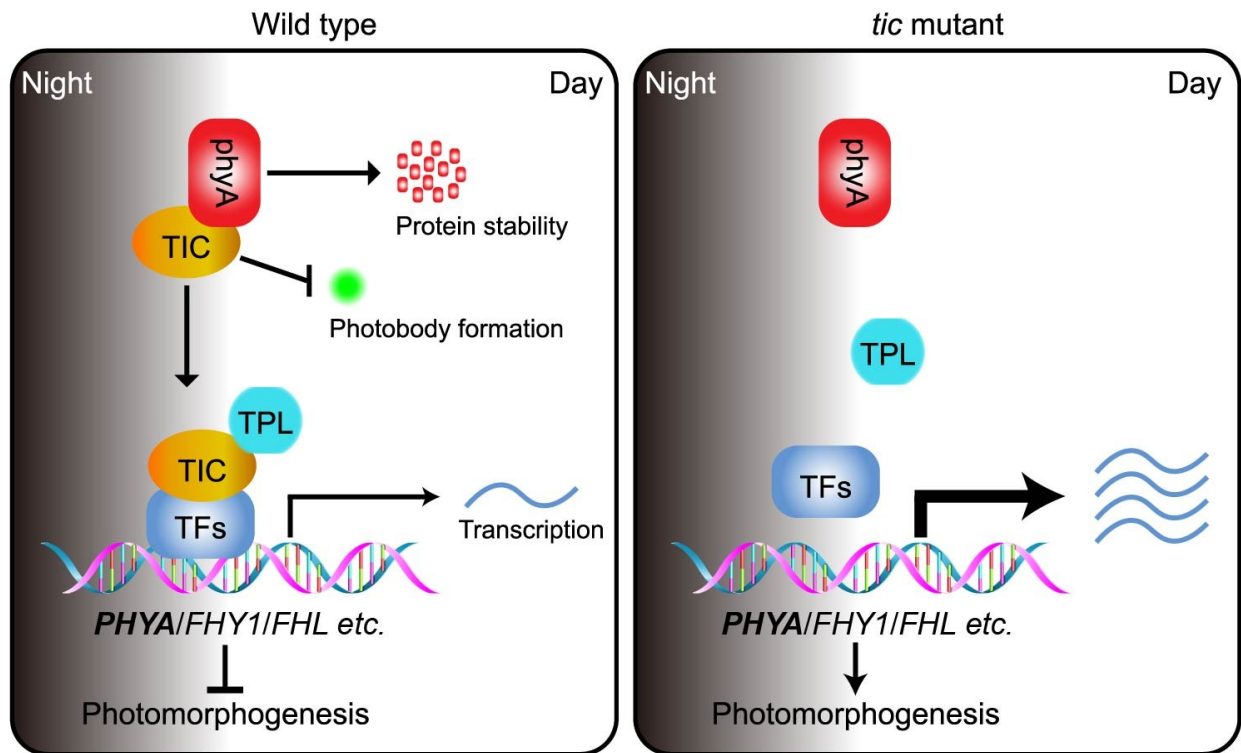
Figure 7. Epistatic relationship between *PHYA* and *TIC*.

105 **(A), (C), and (E)** Hypocotyl phenotypes of Col-0, *tic-2*, *phyA-211*, and *tic-2 phyA-211*. The indicated seedlings were grown under far red light (FR $\sim 0.1, 0.3, 0.5,$ and $1 \mu\text{mol m}^{-2}\text{s}^{-1}$), red light (R $\sim 5, 10, 20,$ and $40 \mu\text{mol m}^{-2}\text{s}^{-1}$) or blue light (B $\sim 1, 5, 10,$ and $20 \mu\text{mol m}^{-2}\text{s}^{-1}$) for 5 days. Representative seedlings are shown in (A), (C), and (E), bars = 5 mm.

110 **(B), (D), and (F)** Quantitative analysis of hypocotyl length of the Col-0, *tic-2*, *phyA-211*, and *tic-2 phyA-211* plants shown in (A), (C) and (E), respectively. Data represent mean \pm s.e.m. ($n \geq 15$), and the lowercase letters indicate significant differences by one-way ANOVA followed by Tukey's honestly significant difference (HSD) test (SPSS Statistics) ($p < 0.01$).



115 **Figure 8. Genetic relationship between *PHYA* and *TIC* in regulating gene expression.** (A-E) Transcript levels of *FHY1* (A), *FHL* (B), *PAR1* (C), *PIL1*(D), and *HB2* (E) in *tic-2*, *phyA-211* and *tic-2 phyA-211* under 12 h L/ 12 h D conditions. Data represent mean \pm s.e.m. from three biological replicates. The gene expression levels were normalized by the geometric mean of *ACT2* and *PP2A* expression.



120

Figure 9. A proposed model depicting the role of TIC in regulating dawn-phased *phyA* activity and hypocotyl growth.

125

TIC recruits the co-repressor TPL and yet unknown transcription factors (TFs) in the nucleus to form a transcription repressive complex, which subsequently represses the expression of a subset of genes including *PHYA* and other hypocotyl related genes (*FHY1*, *FHL*, and so on) in the morning. Meanwhile, TIC directly interacts with *phyA* to facilitate its proteolysis. By integrating both transcriptional and post-translational mechanisms, TIC finely regulates hypocotyl growth in response to light signals.